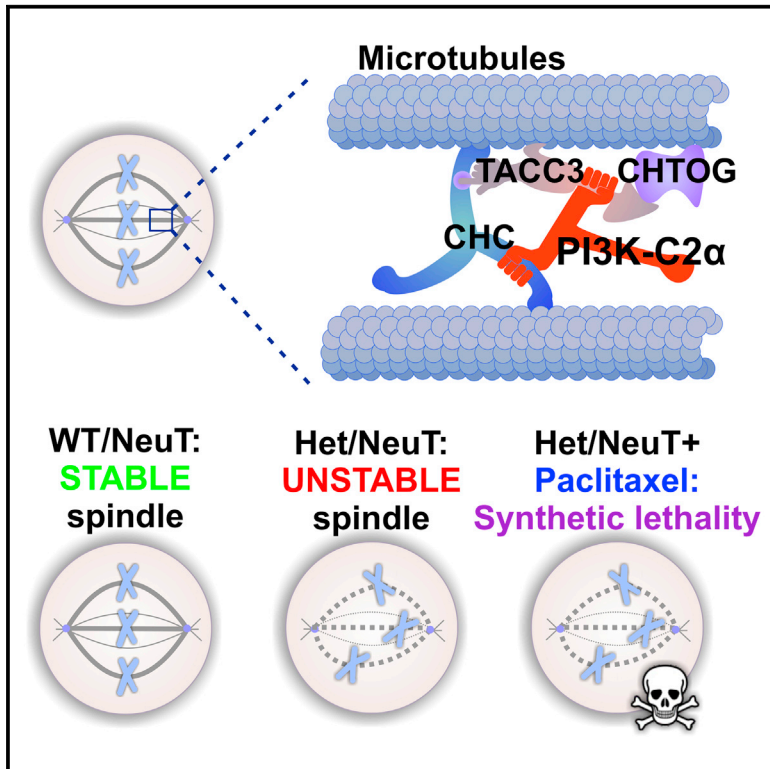# Cancer Cell

Mitotic Spindle Assembly and Genomic Stability in Breast Cancer Require PI3K-C2α Scaffolding Function

Graphical Abstract

Authors

Federico Gulluni, Miriam Martini,
Maria Chiara De Santis, ...,
Roberto Chiarle, Pier Paolo Di Fiore,
Emilio Hirsch

Correspondence

miriam.martini@unito.it (M.M.),
emilio.hirsch@unito.it (E.H.)

In Brief

Gulluni et al. reveal a kinase-independent scaffolding function of PI3K-C2α that affects mitotic spindle formation. Reduced levels of PI3K-C2α reduce tumor growth initially but provide a growth advantage later in mouse models of breast cancer. Loss of PI3K-C2α also increases sensitivity of tumors to taxanes.

Highlights

- The scaffold activity of PI3K-C2α controls spindle stability

- Low PI3K-C2α initially impairs tumor onset but later accelerates cancer growth

- Low of PI3K-C2α is synthetic lethal with taxane-based treatments

- Low PI3K-C2α associates with sensitivity to taxane-based therapy in breast cancer

CrossMark

CellPress

Cell**Press**

Mitotic Spindle Assembly and Genomic Stability in Breast Cancer Require PI3K-C2α Scaffolding Function

Federico Gulluni,[1,14] Miriam Martini,[1,14,*] Maria Chiara De Santis,[1,14] Carlo Cosimo Campa,[1] Alessandra Ghigo,[1] Jean Piero Margaria,[1] Elisa Ciraolo,[1] Irene Franco,[1] Ugo Ala,[1] Laura Annaratone,[2,3] Davide Disalvatore,[4] Giovanni Bertalot,[5] Giuseppe Viale,[6,7] Anna Noatynska,[8] Mara Compagno,[1,9] Sara Sigismund,[4] Filippo Montemurro,[10] Marcus Thelen,[11] Fan Fan,[12] Patrick Meraldi,[8] Caterina Marchiò,[2,3] Salvatore Pece,[5,7] Anna Sapino,[2,13] Roberto Chiarle,[1,9] Pier Paolo Di Fiore,[4,5,7] and Emilio Hirsch[1,15,*]

[1]Molecular Biotechnology Center, Department of Molecular Biotechnology and Health Sciences, University of Torino, Turin 10126, Italy
[2]Department of Medical Sciences, University of Torino, Turin, Italy
[3]Pathology Unit, Department of Laboratory Medicine, Azienda Ospedaliera Universitaria Città della Salute e della Scienza di Torino, Turin, Italy
[4]IFOM, The FIRC Institute for Molecular Oncology Foundation, Milan, Italy
[5]Program of Molecular Medicine, IEO, European Institute of Oncology, Milan, Italy
[6]Division of Pathology, European Institute of Oncology, Milan, Italy
[7]Department of Oncology and Hemato-oncology (DIPO), University of Milan, Milan, Italy
[8]Department of Cell Physiology and Metabolism, University of Geneva, Geneva, Switzerland
[9]Department of Pathology, Boston Children's Hospital and Harvard Medical School, Boston, MA, USA
[10]Unit of Investigative Oncology, Candiolo Cancer Institute - FPO, IRCCS, Candiolo (TO), Italy
[11]Institute for Research in Biomedicine, Università della Svizzera Italiana, Bellinzona, Switzerland
[12]Department of Biological Science and Bioengineering, Key Laboratory of Biomedical Information Engineering of Ministry of Education, School of Life Science and Technology, Xi'an Jiaotong University, Xi'an, Shaanxi, P. R. China
[13]Unit of Pathology, Candiolo Cancer Institute - FPO, IRCCS, Candiolo (TO), Italy
[14]These authors contributed equally
[15]Lead Contact
*Correspondence: miriam.martini@unito.it (M.M.), emilio.hirsch@unito.it (E.H.)
http://dx.doi.org/10.1016/j.ccell.2017.09.002

SUMMARY

Proper organization of the mitotic spindle is key to genetic stability, but molecular components of inter-microtubule bridges that crosslink kinetochore fibers (K-fibers) are still largely unknown. Here we identify a kinase-independent function of class II phosphoinositide 3-OH kinase α (PI3K-C2α) acting as limiting scaffold protein organizing clathrin and TACC3 complex crosslinking K-fibers. Downregulation of PI3K-C2α causes spindle alterations, delayed anaphase onset, and aneuploidy, indicating that PI3K-C2α expression is required for genomic stability. Reduced abundance of PI3K-C2α in breast cancer models initially impairs tumor growth but later leads to the convergent evolution of fast-growing clones with mitotic checkpoint defects. As a consequence of altered spindle, loss of PI3K-C2α increases sensitivity to taxane-based therapy in pre-clinical models and in neoadjuvant settings.

INTRODUCTION

Phosphatidylinositol 3-kinases (PI3Ks) are enzymes producing 3-OH phosphorylated phosphoinositide second messengers and are involved in several processes such as proliferation, sur-

vival, and metabolism (Vanhaesebroeck et al., 2010). PI3Ks are subdivided into three classes with PI3Kα, PI3Kβ, PI3Kδ, and PI3Kγ belonging to class I, PI3K-C2α, PI3K-C2β, and PI3K-C2γ to class II, and Vps34 to class III. Whereas the role of class I PI3Ks in proliferation and cancer is well established, little

Significance

A mainstay of breast cancer neoadjuvant treatment is the combination of taxanes and anthracyclines. Given that not all patients are equally sensitive to each of the two drugs, markers are needed for a safer, more effective precision medicine. Our study shows that low PIK3C2A/PI3K-C2α expression is associated with the loss of a scaffold function stabilizing kinetochore fibers, the taxane targets. In breast cancer models, low PI3K-C2α caused spindle abnormalities and genomic instability, eventually promoting the evolution of fast-growing clones with weakened spindle assembly checkpoint. Invariably, these clones retained abnormal spindles, which resulted in high responsiveness to taxanes independently of known breast cancer subsets. Overall, these observations will open the way to more accurate patient stratification in neoadjuvant regimens.

CrossMark
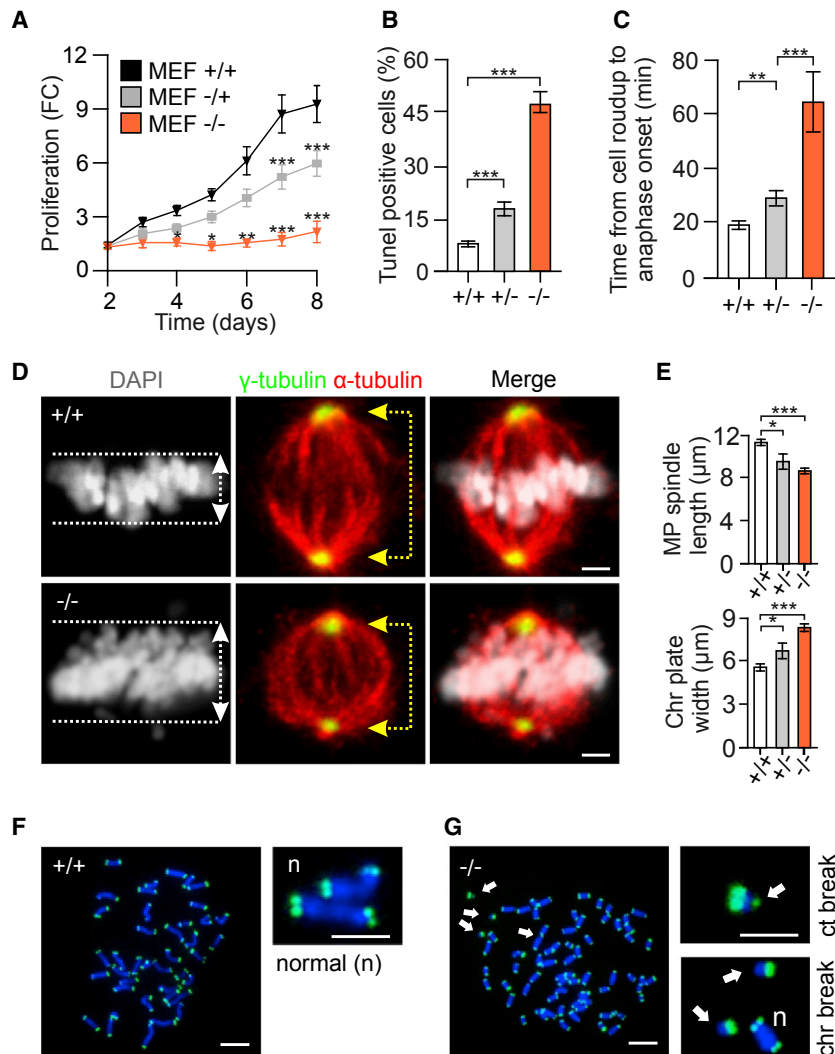
Figure 1. PI3K-C2α Haploinsufficiency Affects Cell Proliferation and Induces Chromosomal Defects

(A) Proliferation curve of freshly isolated wild-type (WT) (MEF +/+), *Pik3c2a*$^{+/-}$ (MEF +/−), and *Pik3c2a*$^{-/-}$ (MEF −/−) MEFs. FC, fold change. Results are shown as mean ± SEM (n = 8).

(B) Apoptosis assay quantification (TUNEL) of freshly isolated WT, *Pik3c2a*$^{+/-}$, and *Pik3c2a*$^{-/-}$ MEFs. Results are shown as mean ± SEM (n = 6).

(C) Time-lapse measurement. Time required to progress from cell roundup to anaphase in freshly isolated WT, *Pik3c2a*$^{+/-}$, and *Pik3c2a*$^{-/-}$ MEFs. Results are shown as mean ± SEM (n = 100 cells).

(D and E) Immunofluorescence (IF) staining of metaphase spindle length and chromosome plate width (D) and relative quantifications (E) in freshly isolated MEFs. Results are shown as mean ± SEM (n = 72 cells). White arrows indicate plate width. Yellow arrows indicate spindle poles (marked by γ-tubulin).

(F and G) Representative images of T-FISH analysis performed in whole metaphase chromosome spreads from freshly isolated +/+ (F) and −/− (G) MEFs. White arrows indicate chromosomal aberrations. Chr, chromosome; ct, chromatide; n, normal.

*p < 0.05, **p < 0.01, ***p < 0.001 by ANOVA followed by Bonferroni's post hoc test. Scale bars, 5 μm. See also Figure S1, Tables S1 and S2, and Movie S1.

interacts with clathrin (Domin et al., 2000; Gaidarov et al., 2005), a protein that controls vesicular trafficking and mitotic spindle stability via two independent mechanisms (Royle, 2013). Whereas clathrin heavy chain (CHC) associates with the clathrin light chain and AP1/2 adaptors on budding membranes during endocytosis, CHC finds other partners to locate at inter-microtubule (MT) bridges in dividing cells during metaphase. CHC is recruited to spindle by the interaction with TACC3, and its loss causes altered chromosome congression and delayed mitotic progression due to reduced kinetochore-MT stability. PI3K-C2α strongly interacts with CHC (Domin et al., 2000; Posor et al., 2013), and this association reflects both its intracellular localization and catalytic activities (Gaidarov et al., 2005). In agreement, proteomic analysis detected PI3K-C2α in the spindle-associated clathrin-TACC3 complex (Hubner et al., 2010).

RESULTS

Loss of PI3K-C2α Impairs Proliferation, Delaying Anaphase Onset

Loss of PI3K-C2α in mice causes embryonic lethality at mid-gestation due to a complex set of different phenotypes, including endothelial disorganization and primary cilium dysfunction (Franco et al., 2014; Yoshioka et al., 2012). Primary mouse embryonic fibroblasts (MEFs) derived from *Pik3c2a*$^{-/-}$ embryos displayed a strongly decreased proliferative capacity (Figure 1A) as well as increased apoptosis (Figure 1B). In line with these

is known about the potential corresponding role of class II enzymes (Campa et al., 2015; Traer et al., 2006). Class II PI3Ks are large molecules ranging from 166 to 190 kDa with the PI3K catalytic core flanked by extended N- and C-terminal arms. Differently from other PI3Ks that function as heterodimers, they do not associate with adaptor proteins. Nonetheless, they participate in complex multimolecular associations through the protein and lipid binding domains contained at their N and C termini. For example, PI3K-C2α and PI3K-C2β can bind clathrin through their N-terminal domains, and this binding is required to enhance the catalytic activity of at least PI3K-C2α (Gaidarov et al., 2001). Our recent work demonstrated that PI3K-C2α has specific non-redundant cellular functions. This enzyme is a key regulator of clathrin-mediated endocytosis (Posor et al., 2013) and of endocytic recycling required for primary cilium function (Franco et al., 2014). While these results highlight the role of PI3K-C2α in vesicular trafficking, increasing evidence is pointing to the importance of class II enzymes in cell proliferation and survival (Elis et al., 2008; Franco et al., 2014, 2015).

Whether and how PI3K-C2α may affect cell-cycle progression and proliferation of cancer cells is still unclear. Of note, PI3K-C2α

observations, time-lapse analysis of cell cycle in freshly isolated *Pik3c2a*$^{-/-}$ MEFs, as well as short hairpin RNA (shRNA)-treated HeLa cells, showed a significant delay in time required to progress from cell roundup to anaphase onset (Figures 1C, S1A, and S1B; Movie S1). Next, the metaphase plate was evaluated in cells treated with MG132 (20 μM) for 2 hr to block mitotic cells in metaphase (Santaguida et al., 2011; Serio et al., 2011). Metaphase spindle length and chromosome plate width were assessed by measuring the distance between γ-tubulin-positive poles and only considering aligned chromosomes (Figures 1D, 1E, and S1C). Loss of PI3K-C2α resulted in altered kineto-chore-MT organization, reduced metaphase spindle length, and increased chromosome plate width (Figures 1D, 1E, and S1C). Heterozygous MEF cells also displayed an intermediate phenotype, suggesting a gene dosage effect (Figures 1A–1C and 1E). This revealed a so far unrecognized role of PI3K-C2α in mitosis, particularly in the chromosomal distribution occurring in metaphase. Therefore, karyotype of mutant cells was analyzed, whereby chromosome counts of *Pik3c2a*$^{-/-}$ MEFs displayed pronounced abnormalities (Table S1). In addition, telomere-fluorescence *in situ* hybridization (T-FISH) analysis showed several chromatid and chromosome breaks in *Pik3c2a*$^{-/-}$ MEF metaphase spreads (Figures 1F and 1G; Table S2). These abnormalities were consistent with disturbed cell division associated with metaphase disorganization (Castedo et al., 2004; Rieder and Maiato, 2004) and suggested that during mitosis, loss of PI3K-C2α alters chromosome congression and segregation, eventually leading to genomic instability.

Reduction of PI3K-C2α Delays Tumor Onset but Promotes Fast-Growing Tumors

In cancer, genomic instability is a crucial driver of tumor evolution, generating phenotypic variation and adaptation under selective pressure (Hanahan and Weinberg, 2011). Thus, the impact of low levels of PI3K-C2α on cancer growth was tested by crossing *Pik3c2a*$^{+/-}$ mice with a transgenic mouse model of mammary carcinogenesis that specifically expresses the activated HER-2/Neu oncogene in the mammary gland (Quaglino et al., 2004). A cohort of *NeuT;Pik3c2a*$^{+/+}$ (wild-type [WT]/NeuT) and *NeuT;Pik3c2a*$^{+/-}$ (Het/NeuT) female mice was followed for about 30 weeks. WT/NeuT animals developed mammary gland tumors by 10 weeks of age with an initial tumor latency of 8 weeks, while Het/NeuT mice showed a significantly delayed tumor latency (16 weeks; p < 0.0001) (Figure 2A). While mammary glands of *Pik3c2a*$^{+/+}$ and *Pik3c2a*$^{+/-}$ 6- to 8-week-old mice appeared structurally identical, Het/Neu showed significantly fewer nodules than WT/Neu (Figure S2A). To evaluate hyperplastic lesions formation, we scored mammary gland ducts of WT/NeuT and Het/NeuT 8-week-old mice into four grades according to lumen fullness (Figure S2B, left panel). In agreement with delayed onset, Het/NeuT mice developed fewer *in situ* carcinomas (Figure S2B, right panel) and showed reduced positive nuclear staining for PCNA (proliferating cell nuclear antigen) compared with control mice (Figure S2C). However, despite the delayed tumor onset, Het/NeuT mice progressively started to develop tumors that grew faster than WT controls (Figures 2B and S2D). At euthanasia, the average number of tumors per mouse was not affected by reduction of PI3K-C2α expression. According their size, tumors were defined as "early" (E)

when the major diameter (D) was <4 mm and "late" (L) when D was >6 mm (see STAR Methods).

Het/NeuT tumors expressed 50% less PI3K-C2α than controls but matching amounts of NeuT protein expression (Figure S2E), confirming that PI3K-C2α and NeuT expression were not affected by tumor size in both genotypes. Furthermore, no alteration in the AKT pathway was detected (Figure S2E). Assessment of proliferation by PCNA staining, in tumors with an average size of 150 mm^3, indicated that Het/NeuT samples display higher positivity than controls (Figure 2C). In addition, TUNEL staining revealed a higher number of apoptotic cells in E than in L Het/NeuT tumors (Figures S2F and S2G). Representative images and relative quantitation of the cellularity (number of nuclei per 20×-power field) of the selected images is provided in Figures S2H and S2I. These results indicate that gene dosage is crucial for PI3K-C2α function and that a reduction of its levels in cancer initially impairs cell proliferation, but in the long run triggers the emergence of fast-growing populations.

Reduced PI3K-C2α Expression Promotes Genomic Instability in Tumor Cell Lines

To define the role of PI3K-C2α in the development of mammary cancer, we generated epithelial cells from primary tumors. Murine mammary epithelial tumor cells (MMET) were derived from E and L, WT/NeuT, and Het/NeuT tumors. Immunostaining with antibodies directed against E-cadherin confirmed the epithelial origin (Figure S2J). Early Het/NeuT MMET confirmed the *in vivo* data, showing an initial decrease in proliferation rate (Figure 2D) and a parallel increase of apoptosis (Figure S2K) followed by the invariable emergence of fast-growing clones (Figure 2E).

To explore the role of PI3K-C2α in chromosomal stability, we analyzed alterations in chromosome congression during metaphase. WT/NeuT and Het/NeuT MMET were treated with MG132 (20 μM) for 2 hr to block mitotic cells in metaphase and the spindle structure was monitored. While chromosomes aligned in a correct equatorial plane position in WT cells, Het/NeuT MMET displayed reduced metaphase spindle length, altered chromosome alignment, and increased metaphase plate width (Figures 2F–2H), in line with what was observed in MEFs and HeLa cells (Figures 1D and S1C). To further validate that loss of PI3K-C2α promotes aneuploidy, we assessed cellular DNA content (ploidy) in MMET cells using fluorescence-activated cell sorting (FACS) analysis. Around 20% of both early WT/NeuT and Het/NeuT MMET showed an aberrant DNA content, likely due to the expression of NeuT, an oncogene sufficient to cause aneuploidy per se (Liu et al., 2002). Of note, the percentage of cells with aberrantly increased DNA content was equal in both early WT/NeuT and Het/NeuT MMET. As expected, late Het/NeuT MMET showed significantly higher aneuploidy than WT controls (Figure 2I). Similar results were obtained by karyotype analysis (Table S3). Taken together, these results demonstrate that PI3K-C2α controls proper metaphase spindle assembly and its loss predisposes to alteration in chromosomes congression/segregation, eventually promoting aneuploidy.

PI3K-C2α Localizes on the Spindle at the Metaphase Stage where It Interacts with TACC3 and CHC

Immunofluorescence analysis of HeLa cells treated with MG132 to prevent mitotic exit revealed that PI3K-C2α is enriched along
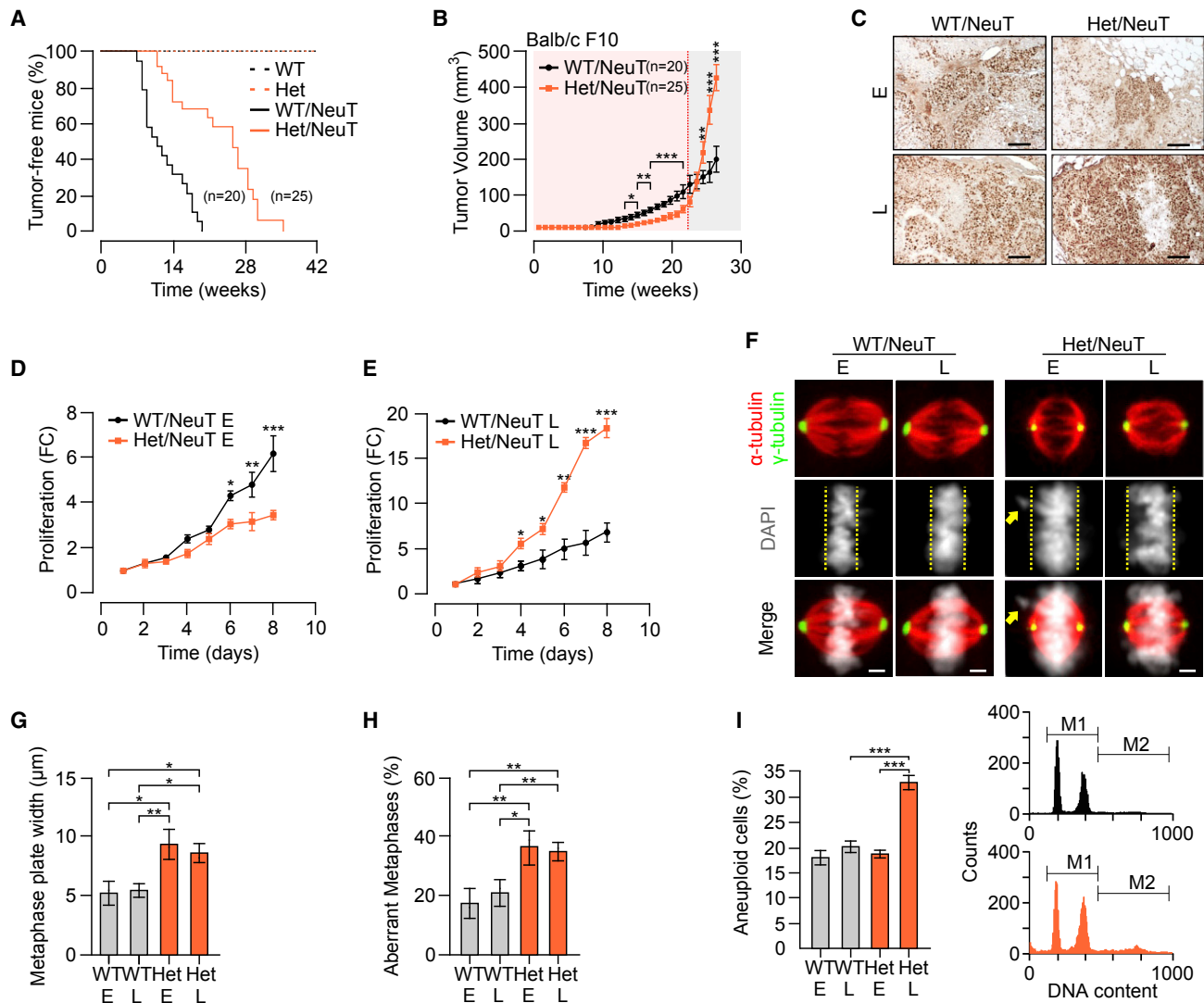
Figure 2. PI3K-C2α Haploinsufficiency Affects Breast Cancer Growth

(A) Kaplan-Meier curve for tumor incidence in *Pik3c2a*^{+/+} (WT), *Pik3c2a*^{+/−} (Het), and NeuT female mice carrying WT (WT/NeuT) or heterozygous deletion of PI3K-C2α (Het/NeuT). n = 20 mice for WT/NeuT and n = 25 mice for Het/NeuT.

(B) Growth curve of WT/NeuT and Het/NeuT tumors in the fourth pair of mammary glands. The red shaded background indicates the early stage of tumors while the gray one the late phase. Results are shown as mean ± SEM (n = 20 mice for WT/NeuT and n = 25 mice for Het/NeuT).

(C) PCNA staining of WT/NeuT and Het/NeuT tumors at early (E) or late (L) stages of development (n = 6). Scale bars, 100 μm.

(D and E) Proliferation curves of WT/NeuT and Het/NeuT MMET derived from E (D) or L (E) stage. FC, fold change. Results are shown as mean ± SEM (n = 8).

(F–H) Analysis of metaphase plate width and aberrant metaphases. IF staining (F), metaphase plate width (G), and aberrant metaphases (H) quantification of E and L WT/NeuT and Het/NeuT MMET. Results are shown as mean ± SD (n = 100 cells). Yellow arrows indicate lagging chromosome in metaphase. Yellow dashed lines indicate the metaphase plate width. Scale bars, 5 μm.

(I) FACS analysis of E and L WT/NeuT and Het/NeuT MMET to score DNA content (propidium iodide staining). M2 gate represents the percentage of aneuploid cells. Results are shown as mean ± SEM (n = 7).

*p < 0.05, **p < 0.01, ***p < 0.001 by ANOVA followed by Bonferroni's post hoc test. See also Figure S2, and Table S3.

the spindle (Figures 3A and S3A). Specificity of the staining was confirmed using either a GFP-tagged PI3K-C2α (Figure 3A, upper panel) or a highly specific antibody (Figures 3A [middle panel] and S3B). Furthermore, such signals disappeared from the spindle after depleting PI3K-C2α in HeLa cells (Figure 3A, lower panel). Western blot analysis also confirmed anti-PI3K-C2α immunoreactivity in mitotic spindle fractions (Figure 3B) isolated from synchronized HeLa cells (Figure S4A). Given the potential presence of PI3K-C2α in the TACC3 interactome (Hubner et al., 2010) together with the existence of a PI3K-C2α/CHC (Domin et al., 2000) and TACC3/CHC association (Cheeseman et al., 2013), interactions of PI3K-C2α in this complex were further investigated. Endogenous TACC3 and CHC co-immunoprecipitated with PI3K-C2α in metaphase-arrested HeLa and MMET cell lines (Figures 3C and 3D). These analyses demonstrated that, at the metaphase stage,
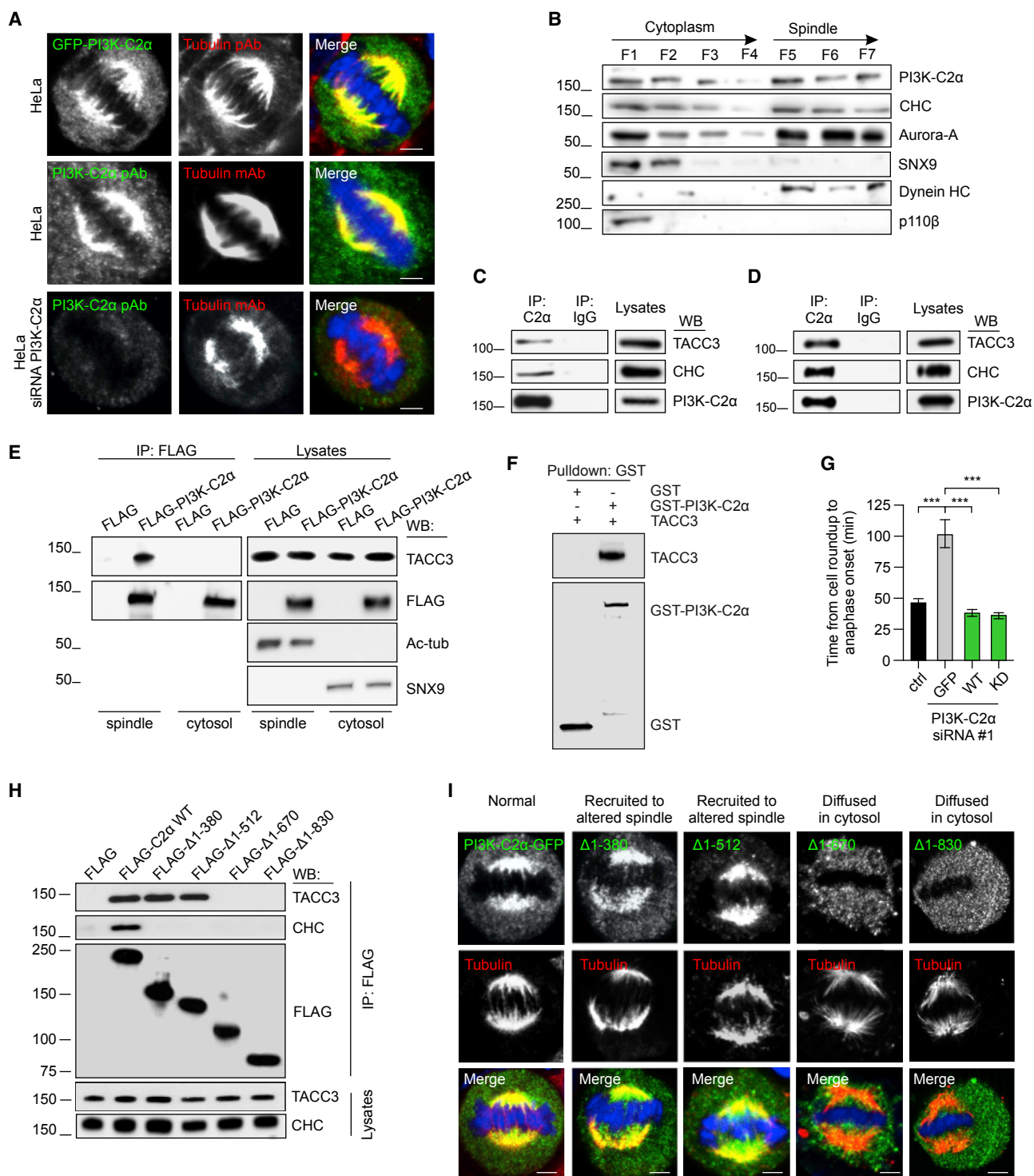
Figure 3. PI3K-C2α Localizes on Metaphase Spindle where It Interacts with TACC3 and CHC

(A) IF staining of PI3K-C2α in HeLa cells. Co-localization of exogenous PI3K-C2α (upper panel, HeLa transfected with GFP-PI3K-C2α) and endogenous PI3K-C2α (middle panel) with α-tubulin (red) on metaphase spindle. HeLa cells stained for PI3K-C2α expression after its siRNA-mediated knockdown (lower panel).

(B) Western blot (WB) analysis of spindle/cytoplasmic fractionation in metaphase-arrested HeLa cells. Whole-cell lysates (WCL) were immunoblotted with indicated antibodies (n = 3).

(C and D) PI3K-C2α was immunoprecipitated (IP) from the cell lysate of metaphase-arrested HeLa (C) or MMET (D) with anti-PI3K-C2α antibody (IP) or control immunoglobulin G. Bound proteins were detected by immunoblotting with anti-TACC3, anti-clathrin heavy chain (CHC), or anti-PI3K-C2α antibody (WB, n = 6).

(legend continued on next page)

PI3K-C2α is an integral component of the TACC3/ch-TOG/ clathrin complex (Booth et al., 2011), interacting with both TACC3 and CHC. Notably, this association was not detected in interphase-arrested HeLa cells (Figure S4B). As shown in Figure 3E, PI3K-C2α–TACC3 interaction occurred preferentially on the spindle-enriched subcellular fraction, as revealed by co-immunoprecipitation (coIP) experiments using HEK293T cells transfected with FLAG-PI3K-C2α. Subsequently, reciprocal control immunoprecipitation confirmed PI3K-C2α–TACC3 association in cells transfected with either TACC3-GFP (Figure S4C) or TACC3-GFP and FLAG-PI3K-C2α (Figure S4D). To further confirm this association, we assessed direct interaction of purified proteins (Figure S4E) in vitro. GST-PI3K-C2α was incubated with purified TACC3 and then affinity purified together on glutathione beads, demonstrating the direct binding between PI3K-C2α and TACC3 proteins (Figure 3F). Taken together, these results revealed that PI3K-C2α is part of a protein complex that includes TACC3 and CHC.

To demonstrate that only the scaffold role of PI3K-C2α is critical for proper progression through mitosis, we performed experiments using the catalytic inactive form of PI3K-C2α (kinase dead [KD] mutant R1251P [Franco et al., 2014]), which is still able to interact with CHC but fails to rescue clathrin-mediated endocytosis (Posor et al., 2013). CoIP experiments using either WT or KD PI3K-C2α demonstrated that the enzymatic function of PI3K-C2α is not required for the interaction with TACC3 (Figure S5A). Immunofluorescence analysis for phosphoinositides (Campa et al., 2015; Ciraolo et al., 2014) also revealed that neither PtdIns(3,4)P$_2$ nor PtdIns(3)P are located on the spindle of metaphase-arrested HeLa cells (Figure S5B).

Additionally, time-lapse analyses were performed on PI3K-C2α-silenced HeLa, transfected with a small interfering RNA (siRNA)-resistant version of WT or KD PI3K-C2α. Although the KD PI3K-C2α (Figure S5C) is not able to rescue the endocytic defect (Franco et al., 2014), both WT and KD PI3K-C2α completely rescued the anaphase onset delay (Figures 3G and S5D), showing that PI3K-C2α kinase activity is not required during the metaphase-to-anaphase transition. Taken together, these results revealed a previously unsuspected kinase-independent function of PI3K-C2α and indicate that the metaphase defect is distinct from impaired endocytosis triggered by a catalytically inactive PI3K-C2α.

To investigate which region of PI3K-C2α is required for spindle binding, we generated a panel of ΔN-end PI3K-C2α truncation mutants (Figure S5C) and tested their interaction with TACC3 and CHC. While PI3K-C2α Δ1-380 and Δ1-512 mutants interacted with TACC3, Δ1-670 and Δ1-830 mutants were unable to bind to TACC3, delineating the region of amino acids (aa) 512–670 as the interacting surface (Figures 3H and S5E). All PI3K-C2α ΔN-end mutants failed to associate with CHC (Figures 3H and S5E), indicating that PI3K-C2α interaction with TACC3 is independent of CHC association. Next, subcellular distribution of truncated mutants was evaluated by immunofluorescence, using WT PI3K-C2α as control. The subcellular localization of Δ1-670 and Δ1-830 mutants was cytosolic with a diffuse pattern, while all the other isoforms were properly recruited to the spindle (Figure 3I). To conclusively demonstrate that this region is responsible for the interaction with TACC3, we generated a GFP fusion with aa 512–670 of PI3K-C2α, comprising the TACC3 binding site (GFP-PI3K-C2α 512–670) (Figure S5C). This fragment was immunoprecipitated with anti-GFP antibodies and incubated with recombinant, FLAG-tagged TACC3. As shown in Figure S5F, the PI3K-C2α 512–670 fragment fused to GFP (but not GFP alone) was able to specifically associate with TACC3. In addition, expression of GFP-PI3K-C2α 512–670 in HeLa cells showed that this TACC3 binding fragment is sufficient to localize to the spindle independent of the binding to CHC (Figure S5G).

PI3K-C2α Interacts with TACC3 and CHC to Form a Single Complex

To investigate the sequence of events that involve PI3K-C2α in the recruitment of CHC and TACC3 at the spindle, we performed immunofluorescence analysis of endogenous TACC3 and CHC on metaphase-arrested cells (Figures 4A–4F and S6A–S6C). While spindle localization of TACC3 was unaffected by the loss of PI3K-C2α in both knockdown HeLa cells and Pik3c2a$^{-/-}$ MEFs (Figures 4A–4C and S6A, respectively), a 75% reduction in CHC spindle levels was observed (Figures 4D–4F and S6B). The decrease of CHC, but not of TACC3, from the spindle of Pik3c2a$^{-/-}$ MEFs (Figures S6A and S6B) and PI3K-C2α-silenced HeLa cells (Figures 4A–4F), indicates that PI3K-C2α connects these two inter-MT-bridge components. To fully elucidate the contribution of PI3K-C2α to the molecular network at the spindle, we downregulated TACC3 expression via siRNA in HeLa cells and evaluated the subcellular localization of PI3K-C2α and CHC by immunofluorescence. As reported in Figures S6C and S6D, downmodulation of TACC3 reduces the spindle-associated levels of both CHC and PI3K-C2α by 78% and 70%, respectively. Lastly, to investigate whether loss of PI3K-C2α affects the recruitment of ch-TOG at the spindle, we performed immunofluorescence analysis of endogenous ch-TOG on metaphase synchronized HeLa cells. As described in Figure S6E, ch-TOG spindle levels are unaffected by the reduction of

(E) HEK293T cells were transfected with FLAG vector or FLAG-PI3K-C2α. FLAG-PI3K-C2α was IP from cytoplasmic or spindle fraction of metaphase-arrested HEK293T cells with anti-FLAG antibody (IP). Bound proteins were detected by immunoblotting with anti-TACC3 and anti-FLAG antibody (WB). Spindle fractionation quality was assessed using anti-acetylated tubulin (spindle fraction) and anti-SNX9 (cytosol fraction) antibody (WB) (n = 6).

(F) In vitro binding assay of equimolar amount of GST-PI3K-C2α or GST and FLAG-TACC3, using anti-GST antibody (Pulldown). Bound proteins were detected by immunoblotting with anti-TACC3 and anti-GST antibody (WB) (n = 5). (G) HeLa cells were transfected with GFP vector, siRNA-resistant GFP-PI3K-C2α, or siRNA-resistant GFP-PI3K-C2α KD mutant PI3K-C2α siRNA#1 to restore the time required to pass from cell roundup to anaphase onset (control cells were transfected with scramble siRNA). Results are shown as mean ± SD (n = 37 cells for WT and n = 29 cells for KD).

(H) HEK293T cells were transfected with FLAG vector or FLAG-PI3K-C2α (WT or indicated deletion mutants). FLAG-PI3K-C2α was IP in metaphase-arrested HEK293T cells with anti-FLAG antibody (IP). Bound proteins were blotted with anti-TACC3, anti-CHC, or anti-FLAG antibody (WB) (n = 6).

(I) IF staining of PI3K-C2α (WT or indicated deletion mutants) in metaphase-arrested HeLa cells (n = 3). HeLa cells were transfected with GFP-PI3K-C2α (WT or indicated mutants) and co-localization with α-tubulin (red) on metaphase spindle was evaluated.

***p < 0.001 by ANOVA followed by Bonferroni's post hoc test. Scale bars, 5 μm. See also Figures S3–S5.
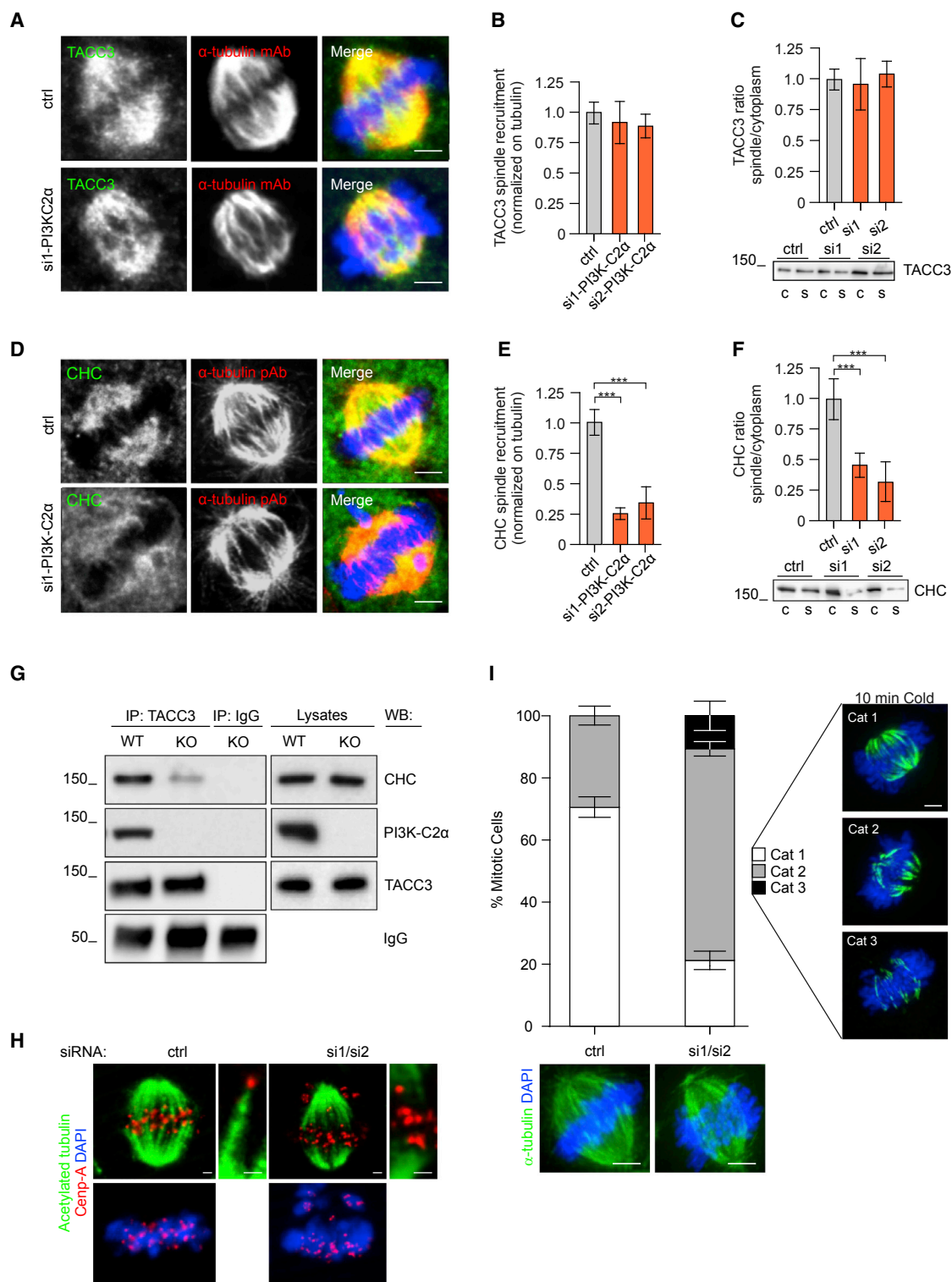
Figure 4. PI3K-C2α Organizes the Mitotic Spindle by Stabilizing the TACC3-CHC Complex

(A–C) Analysis of TACC3 localization. IF staining (A), relative quantification (B), and WB analysis (C) of TACC3 localization on metaphase spindle and cytosolic fraction in control and PI3K-C2α-silenced HeLa cells. Results are shown as mean ± SEM (IF, n = 200 cells; WB, n = 5).

(D–F) Analysis of CHC localization. IF staining (D), relative quantification (E), and WB analysis (F) of CHC localization on metaphase spindle and cytosolic fraction of WT and PI3K-C2α-silenced HeLa cells. Results are shown as mean ± SEM (IF, n = 200 cells; WB, n = 5).

(legend continued on next page)

PI3K-C2α, indicating that ch-TOG spindle localization is unaffected by PI3K-C2α.

Next, the effect of PI3K-C2α downregulation on TACC3/ch-TOG/clathrin complex was evaluated. A coIP experiment was performed in mitotic arrested HEK293T cells where the expression of PI3K-C2α was disrupted using CRISPR/Cas9 technology. The loss of PI3K-C2α expression decreased the interaction between CHC-TACC3 (Figure 4G), supporting the idea that PI3K-C2α can stabilize the complex. To explore the effect of the loss of clathrin in the TACC3/ch-TOG/clathrin complex formation, we used HeLa cells stably expressing an inducible shRNA against CHC (Sorrentino et al., 2013). Formation of the TACC3/ch-TOG/clathrin complex was analyzed in cells that, after doxycycline treatment, showed >80% reduction of CHC protein. In line with a direct PI3K-C2α/TACC3 association, reduction of CHC did not affect the interaction between PI3K-C2α and TACC3 (Figure S6F).

Loss of TACC3/ch-TOG/clathrin complex is known to compromise the metaphase spindle stability due to destabilization of K-fibers (Cheeseman et al., 2013). Since tubulin acetylation and sequential detyrosination are together considered as markers of MT stability, the effects of PI3K-C2α loss were determined by assessing the post-translational modifications of tubulin. Western blot analysis showed reduced level of the ratio between acetylated and tyrosinated tubulin in the spindle fraction of metaphase-arrested MMET and PI3K-C2α-depleted HeLa cells (Figures S6G and S6H).

Reduction of PI3K-C2α caused a significant alteration of the ratio between acetylated and tyrosinated tubulin and suggested a destabilization of spindle MT. In addition, subcellular distribution of acetylated tubulin revealed a missing interaction with kinetochores in mitotically arrested PI3K-C2α-silenced HeLa cells (Figure 4H).

To test for changes in the stability of inter-MT bridges, we incubated control or PI3K-C2α-depleted HeLa cells for 10 min on ice, a condition known to depolymerize astral MTs (Salmon and Begg, 1980). After staining for the remaining kinetochore-MTs by immunofluorescence, spindles were classified into three categories (Amaro et al., 2010; Bird and Hyman, 2008; Gassmann et al., 2010; Vitre et al., 2014): intact mitotic spindles (category 1), partially depolymerized spindles (category 2), and severely depolymerized spindles (category 3, Figure 4I). While control depleted cells contained over 70% of intact spindles, the typical PI3K-C2α-depleted cells with wide spindles contained only 21% intact spindles, 68% partially depolymerized spindles, and 10% severely depolymerized spindles (Figure 4I). These data support the hypothesis that PI3K-C2α depletion destabilizes inter-MT bridges.

Taken together, our results demonstrate that PI3K-C2α is a member of the TACC3/ch-TOG/clathrin complex, controlling MT stability during metaphase.

PI3K-C2α-Deficient Cells Weaken Mitotic Checkpoint by Aberrant Deregulation of Spindle Assembly Checkpoint Genes

Loss of PI3K-C2α expression appears to drive aneuploidy and lead to a highly reproducible emergence of fast-growing cells *in vitro* and *in vivo*. During the first two passages a reduced number of cell doubling was observed in *Pik3c2a*$^{-/-}$ MEFs but not in WT controls. Afterward, a population of proliferating *Pik3c2a*$^{-/-}$ MEFs emerge, which rapidly increased and replaced the pre-existing cell population (Figure S7A). This highlighted the convergent evolution of mutant cells that bypassed the requirement of PI3K-C2α in proliferation and rescued the anaphase onset delay, despite the persistence of aberrant metaphases (Figures 5A–5C).

Profiling of WT/NeuT and Het/NeuT MMET (early and late stages) was performed using real-time PCR to identify and track the expression changes of spindle assembly checkpoint (SAC) genes. Late Het/NeuT tumor cells revealed recurrent abnormal expression of SAC genes, such as Cdc20 and Mad1/2 (Meraldi et al., 2004), but not of other cell-cycle controllers such as cyclin B and p53 (Figures 5D and S7B–S7G). In addition, overexpression of Bub1 kinase was also detected (Figures S7B, S7C, and S7F) but this likely did not breach the mitotic checkpoint, as this is considered a proliferation-dependent phenomenon, correlating with the increased mitotic index (Ricke et al., 2011; van 't Veer et al., 2002). To demonstrate that inactivation of MAD genes is sufficient to overcome proliferation defects in early tumor cells, we studied siRNA-mediated knockdown of MAD1 and MAD2 in early WT/NeuT and Het/NeuT MMET. Downregulation of MAD1/2 was able to recover the proliferation defect in early Het/NeuT MMET with negligible effects in WT cells (Figure S7H).

To directly test for the SAC status, we treated late WT/NeuT and Het/NeuT MMET cells with low (230 nM) and high (5 μM) doses of nocodazole, an MT-interfering drug known to elicit an SAC-dependent anaphase delay (Santaguida et al., 2010) and to prevent all microtubule polymerization at the highest dose (5 μM, Figure S7I). Time-lapse analysis showed that nocodazole delayed early WT and heterozygous MMET (Table S4). The duration of mitosis in late heterozygous MMET cells was 15% or 23% shorter than in WT MMET, respectively, indicating a weakening of the SAC function (Figure 5E and Table S4).

To demonstrate that slow growth in early *Pik3c2a*$^{-/-}$ MEFs was due to a delayed satisfaction of the SAC, we treated cells with NMS-P715, an inhibitor of the SAC kinase Mps1 (Colombo et al., 2010; Koch et al., 2016). Administration of the drug triggered a rapid anaphase entry in mutant early MEFs (Figure 5F) and rescued their cell proliferation defect (Figure S7J), leading to a condition similar to that observed in fast-growing adapted *Pik3c2a*$^{-/-}$ MEFs. In contrast, Mps1 inhibition in fast-growing adapted *Pik3c2a*$^{-/-}$ MEFs did not accelerate anaphase entry, consistent with the absence of a functional SAC in these cells.

(G) HEK293T were transfected with CRISPR/Cas9 KO plasmid targeting *PIK3C2A* gene (KO). After clone isolation, TACC3 was IP with anti-TACC3 antibody (IP). Bound proteins were blotted with anti-CHC, anti-TACC3, or anti-PI3K-C2α antibody (WB) (n = 6).

(H) IF staining of acetylated tubulin (green), Cenp-A (red), and DAPI (blue) in control and PI3K-C2α-silenced HeLa cells (n = 3).

(I) Quantification of kinetochore-MT stability. Stacked bar graph indicates the percentage of the three different morphological categories exemplified on the right in control or PI3K-C2α-depleted HeLa cells. Results are shown as mean ± SEM of calculated percentage (n = 47 cells).

***p < 0.001 by ANOVA followed by Bonferroni's post hoc test. Scale bars, 5 μm. See also Figure S6.
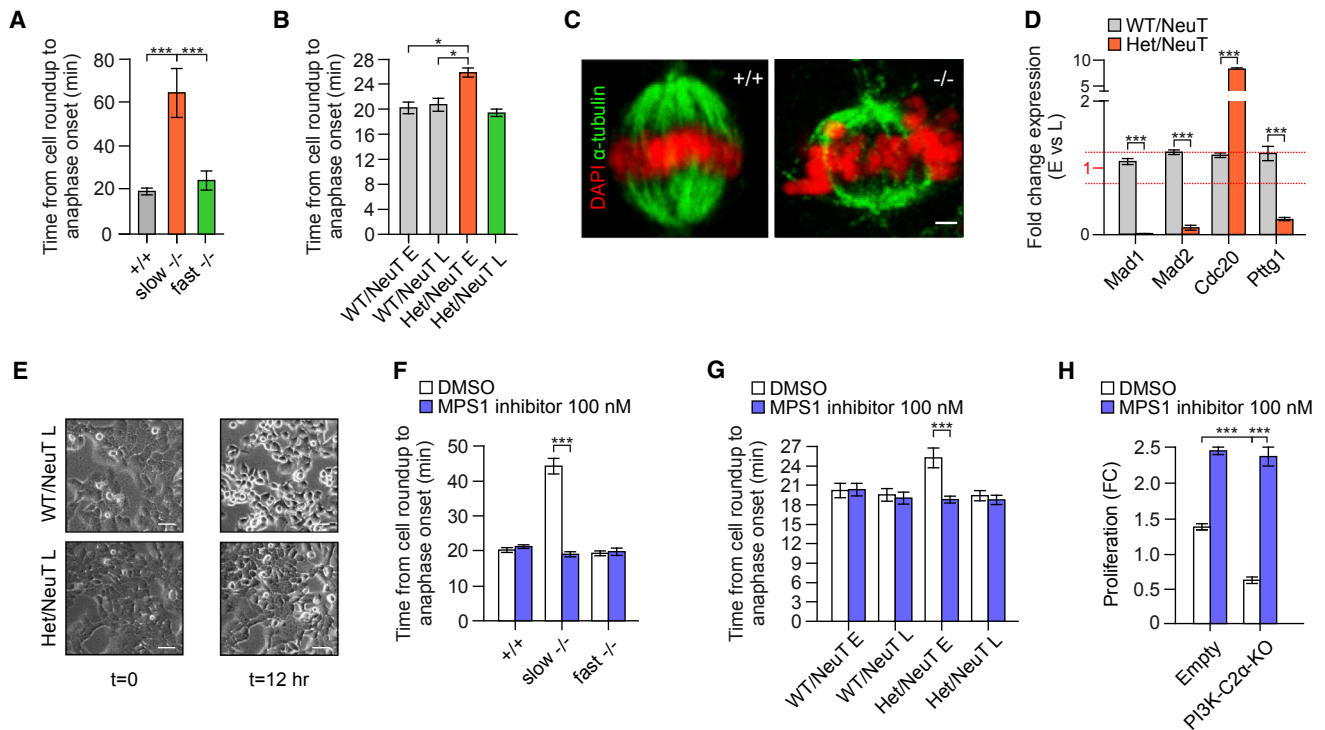
Figure 5. Candidate Genes of the SAC Bypass Metaphase Defect in PI3K-C2α-Deficient Cells

(A and B) Time required to progress from cell roundup to anaphase in WT, early, and fast-growing adapted *Pik3c2a*⁻/⁻ MEFs (A) and MMET cells (B). Results are shown as mean ± SD (n = 100 cells).

(C) IF staining of WT and fast-growing adapted *Pik3c2a*⁻/⁻ MEFs metaphases (n = 5). Scale bar, 5 μm.

(D) Real-time qPCR analysis of expression of SAC-related genes in MMET cells. Results are shown as mean ± SD (n = 5).

(E) Representative images of late, fast-growing WT and Het/NeuT MMET cells treated with 5 μM nocodazole for 12 hr. Scale bars, 60 μm.

(F and G) Effect of spindle assembly checkpoint kinase MPS1 (MPSi) inhibitor on the time required to progress from cell roundup to anaphase on WT and *Pik3c2a*⁻/⁻ MEFs (F) and MMET (G). Results are shown as mean ± SEM (n = 200 cells).

(H) Effect of spindle assembly checkpoint kinase MPS1 (MPSi) inhibitor on MCF10A after *PIK3C2A* CRISPR/Cas9-targeted deletion. Data are normalized on untreated empty MCF10A cells after 48 hr. Results are shown as mean ± SEM (n = 5).

*p < 0.05, ***p < 0.001 by ANOVA followed by Bonferroni's post hoc test. See also Table S4.

Comparable results were obtained by treating with the Mps1 inhibitor early Het/NeuT MMET (Figures 5G and S7K) as well as human breast epithelial cells MCF10A carrying a CRISPR/Cas9-mediated knockout of the *PIK3C2A* gene (Figures 5H and S7L). Taken together, these data demonstrate that the reduction of PI3K-C2α prevents SAC satisfaction and, in the long run, promotes the selection of fast-growing clones with a weakened SAC (Figures S7M–S7O and Movie S2).

PI3K-C2α Is a Synthetic Lethal Partner of Taxane-Based Treatments

Despite the changes in SAC strength, both early and late heterozygous MMET maintained spindle abnormalities (Figure 2F). This suggested that they could become more sensitive than WT controls to anti-MT drugs such as paclitaxel (Gascoigne and Taylor, 2009). As shown in Figure 6A, E and L MMET showed a significantly reduced survival when treated with doses of paclitaxel below 100 nM and known to specifically target MT dynamics (Derry et al., 1995; Jordan et al., 1993). Reintroduction of the WT protein (Figure 6A) in both E and L Het/NeuT MMET cells reduced the action of paclitaxel without affecting the response

to other chemotherapeutic agents used in breast cancer in combination with taxanes, such as doxorubicin (Figure 6B). The increased sensitivity to paclitaxel was also reversed in heterozygous cells rescued with KD PI3K-C2α, thus demonstrating that the catalytic activity of PI3K-C2α is not involved in this effect (Figure 6A). In addition, paclitaxel was equally more effective in both early and late Het/NeuT cells, suggesting that only the loss of PI3K-C2α, but not of SAC function, is linked to the improved response to the drug. Similar results were obtained *in vivo* whereby late Het/NeuT MMET, orthotopically transplanted in syngeneic mice, displayed increased sensitivity to paclitaxel than WT controls (Figure 6C). Heterozygous loss of PI3K-C2α did not enhance sensitivity to anthracyclines alone or in combination with paclitaxel (Figure 6C).

Next, the effect of Taxol on the mitotic spindle was studied in L MMET cells. While in WT/NeuT cells treatment with paclitaxel caused the expected 54% reduction in the number of cells with normal chromosomal alignment (Chen and Horwitz, 2002), in Het/NeuT the same treatment led to a 93% decrease, further confirming an additive effect on spindle microtubule stability triggered by the combination of PI3K-C2α loss and taxanes.
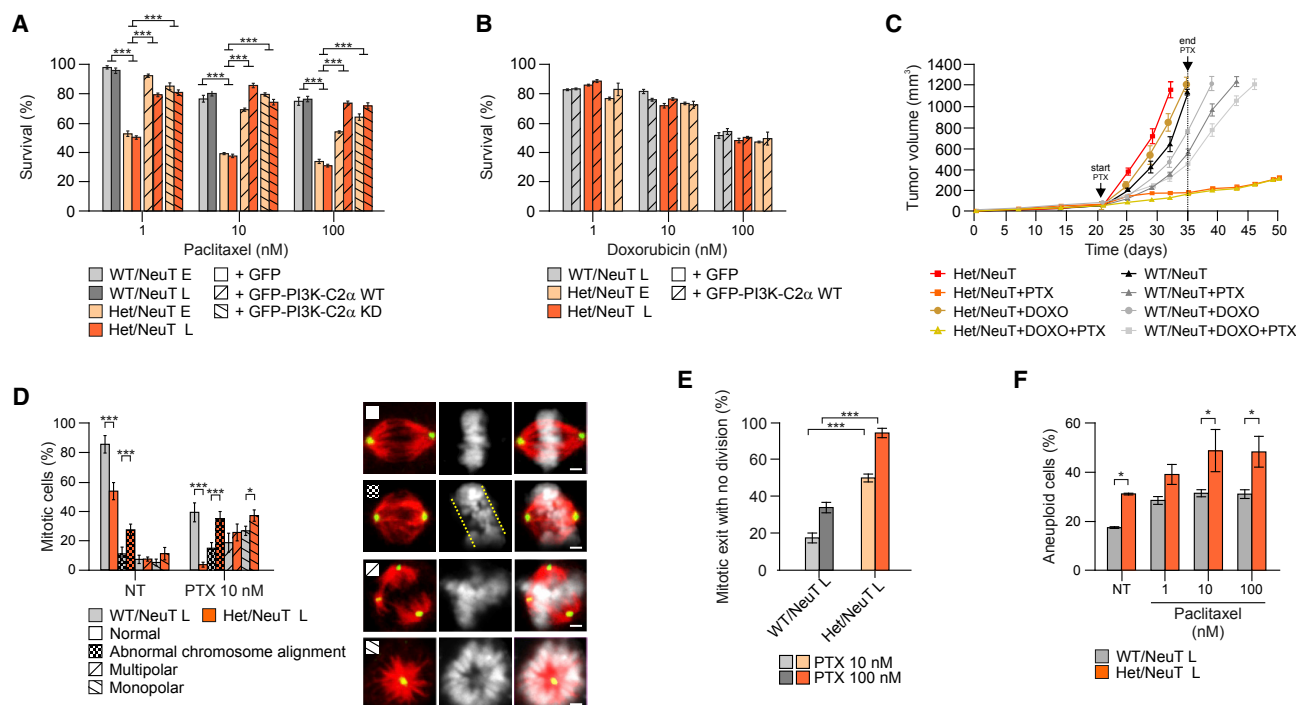
Figure 6. PI3K-C2α Is a Synthetic Lethality Partner of Taxane-Based Treatment

(A) Effect of paclitaxel (PTX) anti-proliferative activity, measured as percent cell survival after treatment, on WT/NeuT and Het/NeuT MMET (plain bars) and rescue experiments with WT or KD PI3K-C2α (dashed bars). Results are shown as mean ± SD (n = 5).

(B) Effect of doxorubicin (DOXO) anti-proliferative activity, measured as percent cell survival after treatment, on WT/NeuT and Het/NeuT MMET (plain bars) and rescue experiments with WT or KD PI3K-C2α (dashed bars) to restore resistance to DOXO treatment. Results are shown as mean ± SD (n = 5).

(C) Effect of PTX, DOXO, or combination of the two drugs (PTX + DOXO) on orthotopic MMET tumors engrafted in syngeneic mice. The treatment was started after 20 days from tumor inoculation (start PTX) and was stopped 15 days later (end PTX). Tumor volume is shown as mean ± SEM (n = 6 mice).

(D) IF analysis of mitotic spindles in WT/NeuT L and Het/NeuT L treated with 10 nM PTX or vehicle only. Spindles where subdivided into four categories (normal, abnormal chromosome alignment, multipolar, and monopolar) and percentage of each category reported in the graph (NT, no treatment). Yellow dashed lines indicate the metaphase plate width. Results are shown as mean ± SD (n = 80). Scale bars, 5 μm.

(E) Time-lapse analysis of late WT/NeuT and Het/NeuT treated with 10 nM or 100 nM of PTX or vehicle only. Percentage of cells exiting mitosis with no division is reported in the graph. Results are shown as mean ± SD (n = 100).

(F) FACS analysis of late WT/NeuT and Het/NeuT MMET to score DNA content (propidium iodide staining) after treatment with PTX (indicated dosage, 24 hr). NT, no treatment. Percentage of cells with aneuploidy is shown as mean ± SEM (n = 5).

*p < 0.05, ***p < 0.001 by ANOVA followed by Bonferroni's post hoc test. See also Figure S7 and Movie S2.

Furthermore, the number of L Het/NeuT MMET cells with abnormal or monopolar chromosomal alignment significantly increased (Figure 6D). As a consequence of enhanced spindle abnormalities, cells that exited mitosis without division at 10 and 100 nM paclitaxel was 65% and 54% higher in heterozygous than WT controls (Figure 6E and S7P). In line with these findings, L Het/NeuT MMET exiting mitosis without division generated a significantly higher number of cells with aberrant DNA content than controls (Figures 6F and S7Q). Therefore, PI3K-C2α loss and paclitaxel additively disturb spindle microtubule structure, eventually enhancing abnormal metaphases, aneuploidy, and cell death.

Role of PI3K-C2α in Human Breast Cancer Models

To assess whether changes in PI3K-C2α levels were associated with human breast cancer, we analyzed publicly available data-sets (Table S5). Data mining revealed that *PIK3C2A* is rarely mutated in breast cancer (<1%), but presents loss of heterozygosity in 22.8% of cases (219 out of 960), a condition more

frequent than deep deletion and/or amplification (Cerami et al., 2012; Gao et al., 2013). This pattern is specific for *PIK3C2A* and is not shared with its closest homolog *PIK3C2B* which, in breast cancer, is more frequently amplified (12.7%) than down-regulated (1%) (Table S5) (Cerami et al., 2012; Gao et al., 2013). Next, PI3K-C2α protein expression was analyzed by IHC on tissue microarrays in a large cohort (1,779 patients) of human breast cancers (Table S5). Low levels of PI3K-C2α were found in ~48% of the patients (IHC score ≤1), while ~52% of the patients were classified as high expressers (IHC score >1). This cutoff (≤1 versus >1, low and high, respectively) was used to stratify patients with respect to indicators of disease recurrence. Stratification of individual patients for their intrinsic likelihood of developing early or late metastasis was based on the commonly used 5-year landmark (Abraham et al., 2010), which likely reflects differences in the molecular mechanisms underlying metastasis in the early and late interval (Dubsky et al., 2013). Hazard ratio (HR) was calculated with both univari-ate and multivariable Cox proportional hazard models with

time-varying covariate. Multivariable models included grade, Ki-67, HER2 status, estrogen/progesterone status, tumor size, number of positive lymph nodes, and age at surgery if available. In the first 5 years, HR was significantly lower in patients with low PI3K-C2α, but this statistically significant difference was lost in the second 5 years of follow-up (Table S5 and Figure S7R). Next, tumors were stratified into the three different subtypes (luminal, HER2, and basal) based on the St. Gallen subtype predictor. HR was then calculated for each of the three molecular subtypes with both univariate and multivariate models. As reported in Table S5, multivariate analysis showed no statistically significant difference in HR between any of the three molecular subtypes.

To define the mechanism of this subtype-independent evolution of PI3K-C2α low breast cancers, we evaluated the effect of the heterozygous loss of PI3K-C2α in a panel of breast cancer cell lines. Given that PI3K-C2α-deficient murine cells bypass proliferative defects by deregulation of mitotic checkpoint, SAC function was tested using nocodazole-induced mitotic arrest (De Antoni et al., 2005; Kim et al., 2010; Qi and Yu, 2007). Analysis of DNA content by FACS staining showed that MCF7 cells, but not SKBR3 cells, displayed a normal SAC function and accumulated in G_2/M in the presence of 100 ng/mL nocodazole. Next, MCF7 were infected with a viral vector able to silence PI3K-C2α expression. Downregulation of PI3K-C2α did not affect SAC function in MCF7 cells, as shown in FACS analysis (Figure 7A). In agreement with what was observed in murine cells, shRNA-mediated downregulation of PI3K-C2α in these cells induced a strong delay in cancer growth in NSG mice (Figure 7B, upper panel). Interestingly, MCF7 tumors clustered into two groups where growth was either completely arrested (n = 6) or showed a biphasic kinetics (n = 4) with an initial delay and the emergence of fast-growing clones (Figure 7B, lower panel). This was not caused by the re-expression of PI3K-C2α after shRNA downregulation (Figure 7C) but by a spontaneous selection of clones with a weakened SAC whereby nocodazole was unable to trigger a G_2/M arrest (Figure 7A, bottom left panel).

To conclusively demonstrate that the evolution of tumors with reduced PI3K-C2α was caused by defects in the mitotic function of the protein, we stably expressed the TACC3 binding fragment of PI3K-C2α in SAC-proficient MCF7 cells (Figure S7S). The GFP-PI3K-C2α 512–670 mutant encompasses the amino acids that bind TACC3 but not those that bind clathrin (Figure S5F). This mutant, which lacks the bridging function of PI3K-C2α (Figure S5C), localizes on the spindle (Figure S5G) and, by definition, cannot harness other PI3K-C2α-mediated functions when expressed in the presence of the endogenous protein. Overexpression of this fragment might thus unleash a dominant-negative effect, interfering with the proper assembly of the TACC3-CHC complex but leaving the other interphase functions of the endogenous PI3K-C2α intact (ratio of internalized to surface transferrin: 1 ± 0.018 and 1.06 ± 0.07 in MCF7 transfected with GFP or GFP-PI3K-C2α 512–670 mutant, respectively). After transfection, proliferation was assessed and found to be significantly reduced (Figure S7T). To demonstrate that SAC weakening is required to overcome the defective mitotic function of PI3K-C2α, we treated MCF7 cells stably expressing GFP-PI3K-C2α 512–670 with the MPS1 inhibitor to mimic SAC defects.

As shown in Figure S7T, the proliferation impairment due to GFP-PI3K-C2α 512–670 expression was rapidly rescued after the administration of the MPS1 inhibitor. To finally demonstrate that the evolution of tumors with reduced PI3K-C2α was caused by defects in the mitotic function of the protein, we kept MCF7 stably expressing the TACC3 binding fragment of PI3K-C2α in culture for a longer time. After 8 weeks of culture, two independent MCF7 clones expressing GFP-PI3K-C2α 512–670 emerged that showed fast growth and SAC weakening (G_2/M: 70.3 ± 1.6 and 32.2 ± 1.1 in nocodazole-treated MCF7 expressing GFP or GFP-PI3K-C2α 512–670, respectively).

This confirmed that the fragment carried a dominant-negative activity unrelated to the "non-mitotic" role of the PI3K-C2α enzyme. Taken together, these data further reinforced the hypothesis that, similarly to the murine model, low PI3K-C2α levels in human breast cancer models delay tumor onset only in the presence of a functional SAC while its reduction, in the long run, leads to the selection of fast-growing clones with a weakened SAC.

Role of PI3K-C2α in Response to Taxane-Based Therapy

Next, the sensitivity to paclitaxel was assessed in a panel of human breast cancer cells in which the expression of PI3K-C2α was downregulated using shRNAs (Table S5). To exclude off-target effects due to shRNA-mediated PI3K-C2α knockdown, we transfected shRNA-resistant PI3K-C2α WT or KD constructs in a panel of human breast cancer cell lines (BT474, MCF7, MDA-MB231, and SKBR3) in which PI3K-C2α expression was knocked down. In all cell lines observed, sensitivity to paclitaxel increased with loss of PI3K-C2α but returned to normal in knockdown cells with the add-back of a KD mutant increased (Figure 7D and Table S5). Similarly to our murine models (Figure 6B), low levels of PI3K-C2α did not affect the response to treatment with anthracyclines usually administered in combination with taxanes (Figure 7D). Finally, increased paclitaxel sensitivity due to PI3K-C2α reduction was tested *in vivo* using cells with a dysfunctional SAC, such as SKBR3 (Figure 7A). As expected, downregulation of PI3K-C2α in SKBR3 cells did not change the rate of tumor growth in NSG mice but increased sensitivity to paclitaxel without affecting the response to the anthracycline doxorubicin (Figure 7E).

To consolidate our pre-clinical results indicating that decreased PI3K-C2α leads to enhanced sensitivity to paclitaxel, we tested the expression of the *PIK3C2A* gene in a cohort of breast cancer patients and correlated this with the response to taxane-based neoadjuvant therapies. Given that protocols based on taxanes alone are deprecated in a neoadjuvant setting, only a very small group of patients was available (n = 40). Remarkably, pathological complete response (pCR) rate was significantly higher in patients with low *PIK3C2A* (22% low *PIK3C2A* versus 4% high *PIK3C2A*, p = 0.04 by chi-square test; Table S5). This group of patients was part of a two-arm clinical trial where 54 or 40 patients received an anthracycline-only or a taxane-only neoadjuvant regimen, respectively (GSE21997). This allowed one to test whether low *PIK3C2A* expression correlated with the response to anthracyclines. In line with our results in cell lines and xenografts, no correlation was found between low *PIK3C2A* expression and pCR to anthracyclines (n = 54, 11% low *PIK3C2A* versus 11% high *PIK3C2A*,
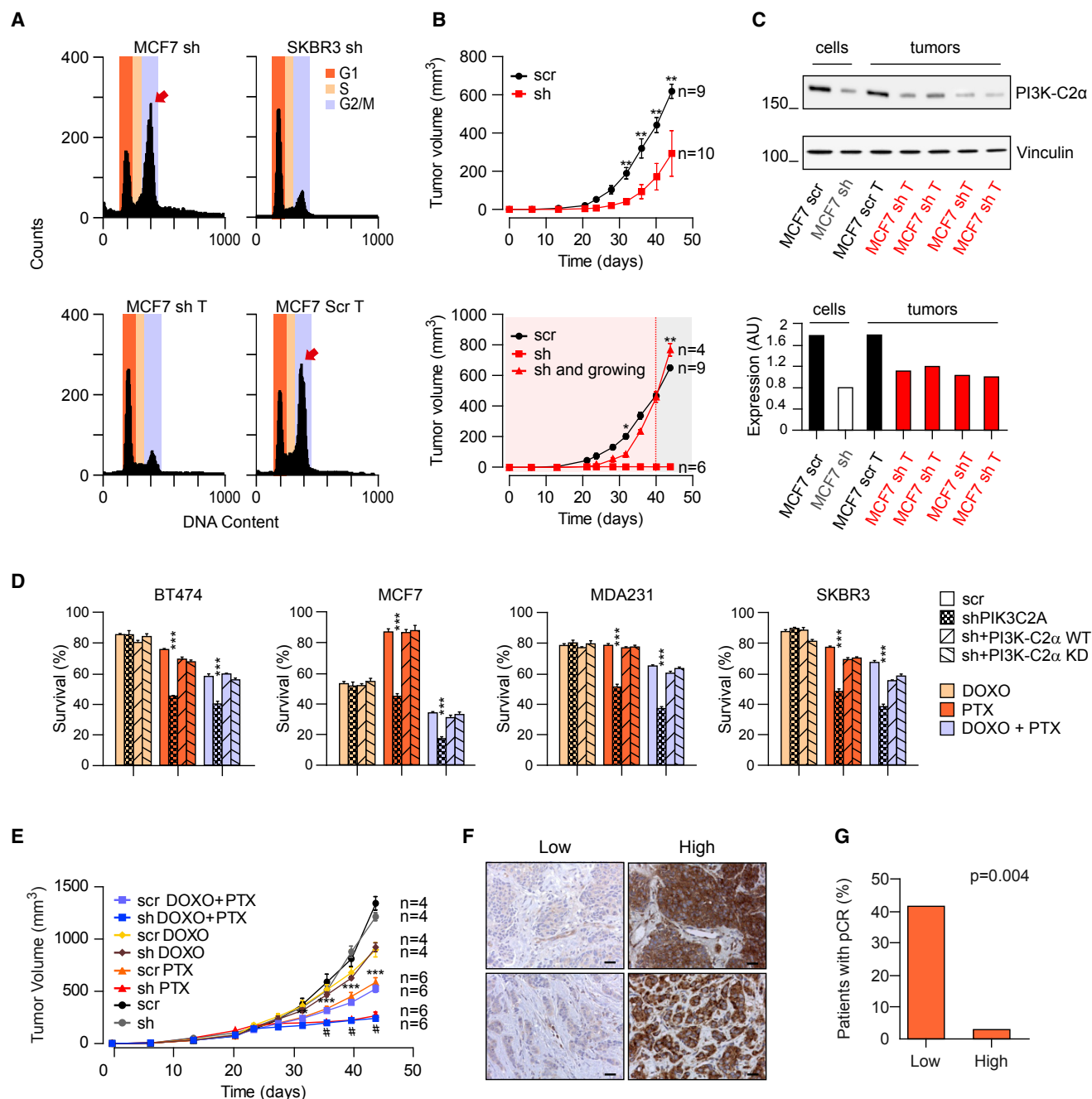
Figure 7. Role of PI3K-C2α in Human Breast Cancer

(A) Propidium iodide staining and FACS analysis of shRNA-PI3K-C2α MCF7 (MCF7 sh), shRNA-PI3K-C2α SKBR3 (SKBR3 sh), shRNA-PI3K-C2α MCF7 derived from explanted tumors (MCF7 sh T) and scramble MCF7 derived from explanted tumors (MCF7 Scr T) treated with 100 ng/mL nocodazole for 16 hr. Red arrows indicates G₂/M peak.

(B) Tumor growth curve of scramble (Scr) and shRNA-PI3K-C2α MCF7 xenografts in NSG mice. Upper graph: tumor volume quantification of scramble (n = 9) versus shRNA (n = 10) MCF7. Lower graph: tumor volume quantification of scramble (circles, n = 9) and shRNA-treated MCF7cells (growth arrested, squares, n = 6; or growing, triangles, n = 4). The red shaded background indicates the early stage of tumors and the gray one the late phase. Results are shown as mean ± SEM.

(C) PI3K-C2α expression was assessed by WB analysis in indicated cell lines and primary tumors. WCL lysates were immunoblotted with indicated antibodies (n = 3).

(D) Cell survival analyses of scramble (Scr), shRNA-PI3K-C2α, sh + PI3K-C2α WT, and sh + PI3K-C2α KD breast cancer cell lines (BT474, MCF7, MDA231, and SKBR3) after incubating with PTX, DOXO, or a combination of the two drugs (PTX + DOXO) for 24 hr. Cell survival was determined by MTT assays as ratio of live cells after treatment compared with live cells treated with vehicle. Results are shown as mean ± SEM (n = 3).

(legend continued on next page)

p = 0.5 by chi-square test; Table S5). On the basis of these findings indicating that the response to anthracyclines does not depend on the expression level of *PIK3C2A*, our analysis was extended to a larger set of four cohorts that received a more standard combination therapy based on both anthracyclines and taxanes. As expected from the improved response to taxanes in low *PIK3C2A* expressers, pCR significantly correlated with low *PIK3C2A* expression (n = 447, 25% low *PIK3C2A* versus 15% high *PIK3C2A*, p = 0.009 by chi-square test; Table S5). Despite the predictive significance of estrogen receptor (ER) status in breast cancer, no statistically significant difference in *PIK3C2A* level was observed in the ER-positive and ER-negative subgroups. Finally, to assess whether findings with RNA expression could be corroborated by analysis of protein abundance, using IHC we analyzed a series of pre-treatment core biopsies from 43 patients from a single-center cohort homogeneously treated with anthracyclines and taxanes and divided them into low (score 0/1; n = 12) and high (score 2/3; n = 31) PI3K-C2α expressers (Figure 7F). In line with the average response to this neoadjuvant treatment (Prowell and Pazdur, 2012), the cohort showed pCR in 13.9% (6/43) of patients. No association was found between PI3K-C2α expression and ER status (Table S5). Consistent with our data *in silico*, pCR was higher in low PI3K-C2α expressers (41.7%; 95% confidence interval = 19%–68%) than in high PI3K-C2α expressers (3.2%; 95% confidence interval = 0.0001%–17%; p = 0.004 by Fisher's exact test; Figure 7G and Table S5), thus indicating that low PI3K-C2α expression significantly correlates with pCR in a taxane-based neoadjuvant chemotherapy.

DISCUSSION

Metaphase-to-anaphase transition is a tightly regulated event in which quality control mechanisms ensure that all chromosomes are correctly attached to the mitotic spindle before anaphase onset. In addition to well-known metaphase players, moonlighting functions in mitosis are emerging since the discovery of the roles of clathrin at the metaphase spindle. The TACC3/ch-TOG/clathrin complex (Booth et al., 2011) is crucial for stabilizing spindle K-fibers by crosslinking adjacent MTs (Cheeseman et al., 2013). Whether endocytosis persists during mitosis is still controversial, and given the established role of PI3K-C2α in clathrin-mediated membrane trafficking, we investigated whether the mitotic role of PI3K-C2α could be dependent on its endocytic function. Previous studies indicate that loss of PI3K-C2α catalytic activity blocks clathrin-coated pit maturation and CHC-mediated endocytosis (Posor et al., 2013). Accordingly, a KD PI3K-C2α mutant cannot rescue the endocytic defect that specifically depends on PI3K-C2α-mediated PtdIns(3,4)P_2 production (Posor et al., 2013). Our results showed that loss of PI3K-C2α leads to a delayed metaphase that could be fully rescued by a KD PI3K-C2α. These observations demonstrate

that the role of PI3K-C2α during metaphase is independent of endocytosis but involves the association with TACC3 at the spindle. Although direct binding between TACC3 and clathrin has been previously suggested (Hood et al., 2013), downregulation or genetic loss of PI3K-C2α reduced the amount of CHC at the mitotic spindle. Our studies with purified proteins clearly demonstrated that PI3K-C2α directly interacts with TACC3, suggesting a tripartite complex with CHC binding both PI3K-C2α and TACC3 but where PI3K-C2α is a key stabilizer. Our findings are not in contrast with the previously identified direct interaction between TACC3 and CHC (Hood et al., 2013) but indicate that, in cultured cells, this interaction is insufficient to fully sustain the organization of the complex when the stabilizing function of PI3K-C2α is lost. In agreement with this view, in the absence of PI3K-C2α, immunoprecipitation of TACC3 pulls down a significantly reduced amount of CHC but does not abolish the CHC/TACC3 complex. In further agreement, the PI3K-C2α CHC binding domain (aa 1–380) and the TACC3 binding site (aa 512–670) reside in two distinct regions of the protein, possibly allowing simultaneous interaction with CHC and TACC3. Moreover, our results indicated that the enrichment of PI3K-C2α at the spindle is mediated by its TACC3 binding site but is CHC independent. We found that TACC3 spindle levels were generally unaffected by the reduction of PI3K-C2α, indicating that PI3K-C2α is not required for TACC3 spindle localization. Although the lack of CHC causes a 10% loss of TACC3 from the spindle (Booth et al., 2011), our data indicate that this small difference was likely lost due to the residual CHC/TACC3 interaction detected in PI3K-C2α knockout cells. Overall, this further corroborates the view that PI3K-C2α acts as a stabilizer of the CHC/TACC3 complex. Downmodulation of TACC3 reduced the spindle-associated levels of both PI3K-C2α and CHC, confirming that PI3K-C2α acts downstream of TACC3 and upstream of CHC. Therefore, the impairment of inter-MT bridges, due to the loss of PI3K-C2α, results in defective K-fiber attachment and delayed mitosis.

In either early MEFs or normal breast cells (MCF10A) lacking PI3K-C2α, the delayed exit from mitosis was completely rescued by the inhibition of MPS1, a key kinase controlling SAC activation, or by MAD2 knockdown. Therefore, the disturbance in spindle organization in cells with reduced/abolished PI3K-C2α expression is sufficient to activate the SAC and delay/block metaphase completion. In line with this view, when SAC is inhibited cells start to proliferate, thus indicating that proliferation is reduced because of SAC activation and not because of an abnormal spindle. In further agreement, spontaneously emerging fast-growing clones weakened the mitotic checkpoint through the deregulation of genes responsible for sensing chromosome binding to K-fibers, including upregulation of Cdc20 and reduced expression of the MAD genes.

While the exact role(s) of PI3K-C2α in cancer remains to be established, the sum of our results in cell culture, in experimental

(E) Effect of PTX (n = 6), DOXO (n = 4), or combination of the two drugs (PTX + DOXO) (n = 6) on tumor growth of scramble (Scr) and shRNA-PI3K-C2α (sh) SKBR3 xenografts in NSG mice (untreated mice n = 4). Results are shown as mean ± SEM.
(F) Immunohistochemical (IHC) assessment of the level of PI3K-C2α expression. Left panel: cases with low staining are scored as IHC score 1. Right panel: cases showing positivity to PI3K-C2α staining (IHC score 3) (×40) (n = 43 patients). Scale bars, 40 μm.
(G) PI3K-C2α and pathological complete response (pCR) after ATx6 chemotherapy regimen (n = 43 patients).
*p < 0.05, **p < 0.01, ***p < 0.001 by ANOVA followed by Bonferroni's post hoc test. See also Table S5.

model systems of tumorigenesis, and in naturally occurring breast cancers argues for a complex impact of PI3K-C2α on the natural history of tumors, which possibly reflects a general physiological role of PI3K-C2α in the control of genomic stability (Hanahan and Weinberg, 2011). The biphasic dependence of tumor growth on the levels of expression of PI3K-C2α is compatible with the possibility that low levels of expression of the protein cause genomic instability, which, in turn, would initially determine an impairment in proliferative fitness but slow progress toward the emergence of aneuploidy and selection of fast-growing clones. An outstanding question is whether breast cancers displaying low levels of PI3K-C2α are actual "underexpressers" and whether this is due to genetic alterations. This issue has not been directly addressed here; however, a survey of available public genomic datasets, through the cBioportal (Cerami et al., 2012; Gao et al., 2013), revealed frequent putative hemizygous deletions in the *PIK3C2A* gene in breast cancers (∼23% of the cases), vis-à-vis rare mutations or putative homozygous deletions or copy gains. Notably, this alteration pattern seems specific for the *PIK3C2A* gene and is not shared with the *PIK3C2B* gene, which is more frequently putatively amplified (20%) than downregulated in breast cancer. Thus, downregulation of *PIK3C2A* expression might randomly occur during breast cancer evolution and provide an initial detrimental effect on cell growth, later compensated by increased aneuploidy eventually leading to cancer progression.

Given the prominent role of PI3K-C2α in controlling MT stability and spindle organization, it is intriguing that a correlation between PI3K-C2α abundance and response to an anti-MT drug, such as paclitaxel, was found. Our pre-clinical data indicate that loss of PI3K-C2α does not influence the response to doxorubicin but enhances Taxol toxicity by further destabilizing kinetochore fibers. Loss of PI3K-C2α increases the number of abnormal metaphases but, in the presence of Taxol (Gascoigne and Taylor, 2009), such abnormalities are further enhanced, thus explaining the increased sensitivity detected in both SAC-proficient and SAC-deficient cells. Mitotic checkpoint dysfunction has been previously related to resistance to taxane-based therapy (Weaver, 2014). However, none of these reports associated a spindle dysfunction with what was observed. Our study shows that increased sensitivity to taxane-based therapies cannot be assumed for all cancers with dysfunctional SAC but that improved taxane efficacy is a consequence of the loss of key components that, like PI3K-C2α, stabilize kinetochore fibers. In agreement with this view, enhanced Taxol sensitivity is shown by cells lacking TACC3, another component of the MT binding complex containing PI3K-C2α (Schmidt et al., 2010). In addition, our study associates a dysfunctional spindle with evolution toward clones with weakened SAC rather than clones that restore the lost spindle function to overcome aberrant metaphase and subsequent growth arrest. Our data thus allow us to infer that increased paclitaxel sensitivity in breast cancer is unique to the condition of reduced PI3K-C2α expression and not to the loss of SAC per se.

Remarkably, patients who received the neoadjuvant protocol, based on the frequent combination of taxanes and anthracyclines, showed that reduced *PIK3C2A*/PI3K-C2α expression is associated with increased pCR. Together with the finding that, in a cohort of breast cancer patients receiving anthracyclines alone, reduced *PIK3C2A* expression did not influence the clinical outcome, our results point to a specifically increased sensitivity to taxane-based therapies in patients with low *PIK3C2A*. Anthracyclines are known to cause long-term side effects such as heart failure, and finding patients who can avoid this treatment is mandatory (Ghigo et al., 2016). Our findings thus suggest that the enhanced sensitivity to taxane-based therapy associated with reduced PI3K-C2α could be exploited to stratify patients for clinical protocols with reduced side effects. In line with this view, a number of studies have explored the possibility to omit anthracyclines as a way to reduce the toxicity load for patients. Taxanes play a pivotal role in these alternative regimens, yet the exact clinical and pathological characteristics of patients who could be spared anthracyclines without compromising efficacy are currently uncertain. Therefore, our findings indicate that PI3K-C2α should be further studied in clinical trials as a potential biomarker to tailor neoadjuvant taxane-based treatments in breast cancer patients.

STAR★METHODS

Detailed methods are provided in the online version of this paper and include the following:

- KEY RESOURCES TABLE
- CONTACT FOR REAGENT AND RESOURCE SHARING
- EXPERIMENTAL MODEL AND SUBJECT DETAILS
  - Animals
  - Human Subjects
  - Cell Lines and Primary Cultures
- METHOD DETAILS
  - Analysis of Mice
  - Histopathological Analysis
  - Cell Culture and Proliferation
  - Cell Synchronization
  - Flow Cytometry Analysis
  - CRISPR/CAS9
  - Plasmids
  - Immunofluorescence
  - Protein Analysis
  - Metaphase Spread Preparation and Telomere-FISH (T-FISH) Analysis
  - Cold-Treatment Stability Assay
  - Breast Cancer Patients
- QUANTIFICATION AND STATISTICAL ANALYSIS
  - General Experimental Approaches
  - Statistical Analysis
  - Gene Expression Data Sets

SUPPLEMENTAL INFORMATION

Supplemental Information includes seven figures, five tables, and two movies and can be found with this article online at http://dx.doi.org/10.1016/j.ccell.2017.09.002.

AUTHOR CONTRIBUTIONS

F.G., M.M., and M.C.d.S. designed and performed research, analyzed data, and wrote the manuscript; C.C.C., A.G., E.C., I.F., C.M., L.A., M.C., F.F., and A.N. performed research and analyzed data; U.A., P.M., R.C., D.D., S.P.,

REFERENCES

Abraham, G., Kowalczyk, A., Loi, S., Haviv, I., and Zobel, J. (2010). Prediction of breast cancer prognosis using gene set statistics provides signature stability and biological context. BMC Bioinformatics *11*, 277.

Amaro, A.C., Samora, C.P., Holtackers, R., Wang, E., Kingston, I.J., Alonso, M., Lampson, M., McAinsh, A.D., and Meraldi, P. (2010). Molecular control of kinetochore-microtubule dynamics and chromosome oscillations. Nat. Cell Biol. *12*, 319–329.

Balmativola, D., Marchio, C., Maule, M., Chiusa, L., Annaratone, L., Maletta, F., Montemurro, F., Kulka, J., Figueiredo, P., Varga, Z., et al. (2014). Pathological non-response to chemotherapy in a neoadjuvant setting of breast cancer: an inter-institutional study. Breast Cancer Res. Treat. *148*, 511–523.

Bird, A.W., and Hyman, A.A. (2008). Building a spindle of the correct length in human cells requires the interaction between TPX2 and Aurora A. J. Cell Biol. *182*, 289–300.

Booth, D.G., Hood, F.E., Prior, I.A., and Royle, S.J. (2011). A TACC3/ch-TOG/clathrin complex stabilises kinetochore fibres by inter-microtubule bridging. EMBO J. *30*, 906–919.

Campa, C.C., Martini, M., De Santis, M.C., and Hirsch, E. (2015). How PI3K-derived lipids control cell division. Front. Cell Dev. Biol. *3*, 61.

Castedo, M., Perfettini, J.L., Roumier, T., Andreau, K., Medema, R., and Kroemer, G. (2004). Cell death by mitotic catastrophe: a molecular definition. Oncogene *23*, 2825–2837.

Cerami, E., Gao, J., Dogrusoz, U., Gross, B.E., Sumer, S.O., Aksoy, B.A., Jacobsen, A., Byrne, C.J., Heuer, M.L., Larsson, E., et al. (2012). The cBio cancer genomics portal: an open platform for exploring multidimensional cancer genomics data. Cancer Discov. *2*, 401–404.

Cheeseman, L.P., Harry, E.F., McAinsh, A.D., Prior, I.A., and Royle, S.J. (2013). Specific removal of TACC3-ch-TOG-clathrin at metaphase deregulates kinetochore fiber tension. J. Cell Sci. *126*, 2102–2113.

Chen, J.G., and Horwitz, S.B. (2002). Differential mitotic responses to microtubule-stabilizing and -destabilizing drugs. Cancer Res. *62*, 1935–1938.

Ciraolo, E., Gulluni, F., and Hirsch, E. (2014). Methods to measure the enzymatic activity of PI3Ks. Methods Enzymol. *543*, 115–140.

Coates, A.S., Winer, E.P., Goldhirsch, A., Gelber, R.D., Gnant, M., Piccart-Gebhart, M., Thurlimann, B., and Senn, H.J. (2015). -Tailoring therapies-improving the management of early breast cancer: St Gallen international expert consensus on the primary therapy of early breast cancer 2015. Ann. Oncol. *26*, 1533–1546.

Colombo, R., Caldarelli, M., Mennecozzi, M., Giorgini, M.L., Sola, F., Cappella, P., Perrera, C., Depaolini, S.R., Rusconi, L., Cucchi, U., et al. (2010). Targeting the mitotic checkpoint for cancer therapy with NMS-P715, an inhibitor of MPS1 kinase. Cancer Res. *70*, 10255–10264.

De Antoni, A., Pearson, C.G., Cimini, D., Canman, J.C., Sala, V., Nezi, L., Mapelli, M., Sironi, L., Faretta, M., Salmon, E.D., and Musacchio, A. (2005). The Mad1/Mad2 complex as a template for Mad2 activation in the spindle assembly checkpoint. Curr. Biol. *15*, 214–225.

Derry, W.B., Wilson, L., and Jordan, M.A. (1995). Substoichiometric binding of taxol suppresses microtubule dynamics. Biochemistry *34*, 2203–2211.

Domin, J., Gaidarov, I., Smith, M.E., Keen, J.H., and Waterfield, M.D. (2000). The class II phosphoinositide 3-kinase PI3K-C2alpha is concentrated in the trans-Golgi network and present in clathrin-coated vesicles. J. Biol. Chem. *275*, 11943–11950.

Dubsky, P., Brase, J.C., Jakesz, R., Rudas, M., Singer, C.F., Greil, R., Dietze, O., Luisser, I., Klug, E., Sedivy, R., et al. (2013). The EndoPredict score provides prognostic information on late distant metastases in ER+/HER2− breast cancer patients. Br. J. Cancer *109*, 2959–2964.

Elis, W., Triantafellow, E., Wolters, N.M., Sian, K.R., Caponigro, G., Borawski, J., Gaither, L.A., Murphy, L.O., Finan, P.M., and Mackeigan, J.P. (2008). Down-regulation of class II phosphoinositide 3-kinase alpha expression below a critical threshold induces apoptotic cell death. Mol. Cancer Res. *6*, 614–623.

Franco, S., Gostissa, M., Zha, S., Lombard, D.B., Murphy, M.M., Zarrin, A.A., Yan, C., Tepsuporn, S., Morales, J.C., Adams, M.M., et al. (2006). H2AX prevents DNA breaks from progressing to chromosome breaks and translocations. Mol. Cell *21*, 201–214.

Franco, I., Gulluni, F., Campa, C.C., Costa, C., Margaria, J.P., Ciraolo, E., Martini, M., Monteyne, D., De Luca, E., Germena, G., et al. (2014). PI3K class II alpha controls spatially restricted endosomal PtdIns3P and Rab11 activation to promote primary cilium function. Dev. Cell *28*, 647–658.

Franco, I., Margaria, J.P., De Santis, M.C., Ranghino, A., Monteyne, D., Chiaravalli, M., Pema, M., Campa, C.C., Ratto, E., Gulluni, F., et al. (2015). Phosphoinositide 3-kinase-C2alpha regulates Polycystin-2 ciliary entry and protects against kidney cyst formation. J. Am. Soc. Nephrol. *27*, 1135–1144.

Fu, J., Bian, M., Xin, G., Deng, Z., Luo, J., Guo, X., Chen, H., Wang, Y., Jiang, Q., and Zhang, C. (2015). TPX2 phosphorylation maintains metaphase spindle length by regulating microtubule flux. J. Cell Biol. *210*, 373–383.

Gaidarov, I., Smith, M.E., Domin, J., and Keen, J.H. (2001). The class II phosphoinositide 3-kinase C2alpha is activated by clathrin and regulates clathrin-mediated membrane trafficking. Mol. Cell *7*, 443–449.

Gaidarov, I., Zhao, Y., and Keen, J.H. (2005). Individual phosphoinositide 3-kinase C2alpha domain activities independently regulate clathrin function. J. Biol. Chem. *280*, 40766–40772.

Gao, J., Aksoy, B.A., Dogrusoz, U., Dresdner, G., Gross, B., Sumer, S.O., Sun, Y., Jacobsen, A., Sinha, R., Larsson, E., et al. (2013). Integrative analysis of complex cancer genomics and clinical profiles using the cBioPortal. Sci. Signal. *6*, pl1.

Gascoigne, K.E., and Taylor, S.S. (2009). How do anti-mitotic drugs kill cancer cells? J. Cell Sci. *122*, 2579–2585.

Gasic, I., Nerurkar, P., and Meraldi, P. (2015). Centrosome age regulates kinetochore-microtubule stability and biases chromosome mis-segregation. Elife *4*, http://dx.doi.org/10.7554/eLife.07909.

Gassmann, R., Holland, A.J., Varma, D., Wan, X., Civril, F., Cleveland, D.W., Oegema, K., Salmon, E.D., and Desai, A. (2010). Removal of Spindly from microtubule-attached kinetochores controls spindle checkpoint silencing in human cells. Genes Dev. *24*, 957–971.

Ghigo, A., Li, M., and Hirsch, E. (2016). New signal transduction paradigms in anthracycline-induced cardiotoxicity. Biochim. Biophys. Acta *1863*, 1916–1925.

Goldhirsch, A., Wood, W.C., Gelber, R.D., Coates, A.S., Thurlimann, B., and Senn, H.J. (2007). Progress and promise: highlights of the international expert consensus on the primary therapy of early breast cancer 2007. Ann. Oncol. *18*, 1133–1144.

Goldhirsch, A., Wood, W.C., Coates, A.S., Gelber, R.D., Thurlimann, B., and Senn, H.J. (2011). Strategies for subtypes—dealing with the diversity of breast cancer: highlights of the St. Gallen international expert consensus on the primary therapy of early breast cancer 2011. Ann. Oncol. *22*, 1736–1747.

Hanahan, D., and Weinberg, R.A. (2011). Hallmarks of cancer: the next generation. Cell *144*, 646–674.

Hatzis, C., Pusztai, L., Valero, V., Booser, D.J., Esserman, L., Lluch, A., Vidaurre, T., Holmes, F., Souchon, E., Wang, H., et al. (2011). A genomic predictor of response and survival following taxane-anthracycline chemotherapy for invasive breast cancer. JAMA *305*, 1873–1881.

Hood, F.E., Williams, S.J., Burgess, S.G., Richards, M.W., Roth, D., Straube, A., Pfuhl, M., Bayliss, R., and Royle, S.J. (2013). Coordination of adjacent domains mediates TACC3-ch-TOG-clathrin assembly and mitotic spindle binding. J. Cell Biol. *202*, 463–478.

Hubner, N.C., Bird, A.W., Cox, J., Splettstoesser, B., Bandilla, P., Poser, I., Hyman, A., and Mann, M. (2010). Quantitative proteomics combined with BAC TransgeneOmics reveals in vivo protein interactions. J. Cell Biol. *189*, 739–754.

Hudis, C.A., Barlow, W.E., Costantino, J.P., Gray, R.J., Pritchard, K.I., Chapman, J.A., Sparano, J.A., Hunsberger, S., Enos, R.A., Gelber, R.D., and Zujewski, J.A. (2007). Proposal for standardized definitions for efficacy end points in adjuvant breast cancer trials: the STEEP system. J. Clin. Oncol. *25*, 2127–2132.

Jordan, M.A., Toso, R.J., Thrower, D., and Wilson, L. (1993). Mechanism of mitotic block and inhibition of cell proliferation by taxol at low concentrations. Proc. Natl. Acad. Sci. USA *90*, 9552–9556.

Kim, S., Sun, H., Ball, H.L., Wassmann, K., Luo, X., and Yu, H. (2010). Phosphorylation of the spindle checkpoint protein Mad2 regulates its conformational transition. Proc. Natl. Acad. Sci. USA *107*, 19772–19777.

Koch, A., Maia, A., Janssen, A., and Medema, R.H. (2016). Molecular basis underlying resistance to Mps1/TTK inhibitors. Oncogene *35*, 2518–2528.

Liu, S., Liu, W., Jakubczak, J.L., Erexson, G.L., Tindall, K.R., Chan, R., Muller, W.J., Adhya, S., Garges, S., and Merlino, G. (2002). Genetic instability favoring transversions associated with ErbB2-induced mammary tumorigenesis. Proc. Natl. Acad. Sci. USA *99*, 3770–3775.

Luo, Y., Ran, J., Xie, S., Yang, Y., Chen, J., Li, S., Shui, W., Li, D., Liu, M., and Zhou, J. (2016). ASK1 controls spindle orientation and positioning by phosphorylating EB1 and stabilizing astral microtubules. Cell Discov. *2*, 16033.

Martin, M., Romero, A., Cheang, M.C., Lopez Garcia-Asenjo, J.A., Garcia-Saenz, J.A., Oliva, B., Roman, J.M., He, X., Casado, A., et al. (2011). Genomic predictors of response to doxorubicin versus docetaxel in primary breast cancer. Breast Cancer Res. Treat. *128*, 127–136.

Meraldi, P., Draviam, V.M., and Sorger, P.K. (2004). Timing and checkpoints in the regulation of mitotic progression. Dev. Cell *7*, 45–60.

Pinder, S.E., and Reis-Filho, J.S. (2007). Non-operative breast pathology. J. Clin. Pathol. *60*, 1297–1299.

Posor, Y., Eichhorn-Gruenig, M., Puchkov, D., Schoneberg, J., Ullrich, A., Lampe, A., Muller, R., Zarbakhsh, S., Gulluni, F., Hirsch, E., et al. (2013). Spatiotemporal control of endocytosis by phosphatidylinositol-3,4-bisphosphate. Nature *499*, 233–237.

Prowell, T.M., and Pazdur, R. (2012). Pathological complete response and accelerated drug approval in early breast cancer. N. Engl. J. Med. *366*, 2438–2441.

Qi, W., and Yu, H. (2007). KEN-box-dependent degradation of the Bub1 spindle checkpoint kinase by the anaphase-promoting complex/cyclosome. J. Biol. Chem. *282*, 3672–3679.

Quaglino, E., Iezzi, M., Mastini, C., Amici, A., Pericle, F., Di Carlo, E., Pupa, S.M., De Giovanni, C., Spadaro, M., Curcio, C., et al. (2004). Electroporated DNA vaccine clears away multifocal mammary carcinomas in her-2/neu transgenic mice. Cancer Res. *64*, 2858–2864.

Ricke, R.M., Jeganathan, K.B., and van Deursen, J.M. (2011). Bub1 overexpression induces aneuploidy and tumor formation through Aurora B kinase hyperactivation. J. Cell Biol. *193*, 1049–1064.

Rieder, C.L., and Maiato, H. (2004). Stuck in division or passing through: what happens when cells cannot satisfy the spindle assembly checkpoint. Dev. Cell *7*, 637–651.

Royle, S.J. (2013). Protein adaptation: mitotic functions for membrane trafficking proteins. Nat. Rev. Mol. Cell Biol. *14*, 592–599.

Salmon, E.D., and Begg, D.A. (1980). Functional implications of cold-stable microtubules in kinetochore fibers of insect spermatocytes during anaphase. J. Cell Biol. *85*, 853–865.

Santaguida, S., Tighe, A., D'Alise, A.M., Taylor, S.S., and Musacchio, A. (2010). Dissecting the role of MPS1 in chromosome biorientation and the spindle checkpoint through the small molecule inhibitor reversine. J. Cell Biol. *190*, 73–87.

Santaguida, S., Vernieri, C., Villa, F., Ciliberto, A., and Musacchio, A. (2011). Evidence that Aurora B is implicated in spindle checkpoint signalling independently of error correction. EMBO J. *30*, 1508–1519.

Schmidt, S., Schneider, L., Essmann, F., Cirstea, I.C., Kuck, F., Kletke, A., Janicke, R.U., Wiek, C., Hanenberg, H., Ahmadian, M.R., et al. (2010). The centrosomal protein TACC3 controls paclitaxel sensitivity by modulating a premature senescence program. Oncogene *29*, 6184–6192.

Serio, G., Margaria, V., Jensen, S., Oldani, A., Bartek, J., Bussolino, F., and Lanzetti, L. (2011). Small GTPase Rab5 participates in chromosome congression and regulates localization of the centromere-associated protein CENP-F to kinetochores. Proc. Natl. Acad. Sci. USA *108*, 17337–17342.

Sorrentino, V., Nelson, J.K., Maspero, E., Marques, A.R., Scheer, L., Polo, S., and Zelcer, N. (2013). The LXR-IDOL axis defines a clathrin-, caveolae-, and dynamin-independent endocytic route for LDLR internalization and lysosomal degradation. J. Lipid Res. *54*, 2174–2184.

Traer, C.J., Foster, F.M., Abraham, S.M., and Fry, M.J. (2006). Are class II phosphoinositide 3-kinases potential targets for anticancer therapies? Bull. Cancer *93*, E53–E58.

van 't Veer, L.J., Dai, H., van de Vijver, M.J., He, Y.D., Hart, A.A., Mao, M., Peterse, H.L., van der Kooy, K., Marton, M.J., Witteveen, A.T., et al. (2002). Gene expression profiling predicts clinical outcome of breast cancer. Nature *415*, 530–536.

Vanhaesebroeck, B., Guillermet-Guibert, J., Graupera, M., and Bilanges, B. (2010). The emerging mechanisms of isoform-specific PI3K signalling. Nat. Rev. Mol. Cell Biol. *11*, 329–341.

Vitre, B., Gudimchuk, N., Borda, R., Kim, Y., Heuser, J.E., Cleveland, D.W., and Grishchuk, E.L. (2014). Kinetochore-microtubule attachment throughout mitosis potentiated by the elongated stalk of the kinetochore kinesin CENP-E. Mol. Biol. Cell *25*, 2272–2281.

Weaver, B.A. (2014). How Taxol/paclitaxel kills cancer cells. Mol. Biol. Cell *25*, 2677–2681.

Yoshioka, K., Yoshida, K., Cui, H., Wakayama, T., Takuwa, N., Okamoto, Y., Du, W., Qi, X., Asanuma, K., Sugihara, K., et al. (2012). Endothelial PI3K-C2alpha, a class II PI3K, has an essential role in angiogenesis and vascular barrier function. Nat. Med. *18*, 1560–1569.

STAR★METHODS

KEY RESOURCES TABLE

REAGENT or RESOURCE	SOURCE	IDENTIFIER
Antibodies		
PCNA	Santa Cruz Biotechnology	Cat. # PC-10 sc-56; RRID:AB_628110
PI3K-C2α	Proteintec	Cat. # 22028-1-AP; RRID:AB_11183760
GFP	This paper	N/A
PI3K-C2α	OriGene	Cat. # TA801690 15H1; RRID:AB_2626037
Acetylated-Tubulin monoclonal	Sigma	Cat. # 6-11B-1; RRID:AB_142598
Acetylated-Tubulin polyclonal	Cell Signaling	Cat. # D20G3; RRID:AB_10544694
PtdIns(3)P	Echelon	Cat. # Z-P003; RRID:AB_427221
PtdIns(3,4)P$_2$	Echelon	Cat. # Z-P034; RRID:AB_427222
TACC3	Abcam	Cat. # ab56595; RRID:AB_2303075
CHC	BD	Cat. # 610499; RRID:AB_397865
PI3K-C2α	BD	Cat. # 611046; RRID:AB_398359
pSer473Ak	Cell Signaling	Cat. # 9271; RRID:AB_329825
E-cadherin	Cell Signaling	Cat. # 14472; RRID:AB_1769622
PTEN	Cell Signaling	Cat. # 9559; RRID:AB_1520859
TACC3	Cell Signaling	Cat. # 8069; RRID:AB_1208566
FLAG	Sigma-Aldrich	Clone M2; RRID:AB_439685
total Akt	Cell Signaling	Cat. # 4685; RRID:AB_2225340
Vinculin	Santa Cruz Biotechnology	Cat. # sc-73614; RRID:AB_1131294
Ch-TOG	Abcam	Cat. # ab86073; RRID:AB_1924889
phospho-Histone H3	Abcam	Cat. # ab47297; RRID:AB_880448
GST	Cell Signaling	Cat. #2624; RRID:AB_2189875
Bacterial and Virus Strains		
pLKO.1-puro	Sigma	Cat. # SHC001
TOP10 chemically competent E.Coli	Thermo Scientific	Cat. # C4040
Biological Samples		
Human breast cancer samples (n=1779)	European Institute of Oncology (IEO) in Milan	N/A
Human breast cancer samples (n=43)	Candiolo Cancer Institute IRCCS, Candiolo	N/A
Chemicals, Peptides, and Recombinant Proteins		
Paclitaxel	Cayman Laboratories	Cat. # 10461
Doxorubicin	Sigma	Cat. # D1515
Nocodazole	Sigma	Cat. # M1404
MG132	Calbiochem	Cat. # 474790
GST-PI3K-C2α	Sigma	Cat. # SRP5330
FLAG-TACC3	OriGene	Cat. # SRP5330
Critical Commercial Assays		
MTT	Sigma	Cat. # 11 465 007 001
Deposited Data		
Raw and analyzed data	This paper	Martin et al., 2011
Raw and analyzed data	This paper	Hatzis et al.,2011
Experimental Models: Cell Lines		
HeLa	ATCC	Cat. # CCL-2
HEK293T	ATCC	Cat. # CRL-3216; RRID:CVCL_0063

(Continued on next page)

REAGENT or RESOURCE	SOURCE	IDENTIFIER
MCF10A	ATCC	Cat. # CRL-10317; RRID:CVCL_0598
MCF7	ATCC	Cat. # HTB-22; RRID:CVCL_0031
BT474	ATCC	Cat. # HTB-20; RRID:CVCL_0179
SKBR3	ATCC	Cat. # HTB-30; RRID:CVCL_0033
T47D	ATCC	Cat. # HTB-133; RRID:CVCL_0553
Experimental Models: Organisms/Strains		
Mouse: BALB/c rHER-2/NeuT	Quaglino et al., 2004	N/A
Mouse: BALB/c *Pik3c2a*$^{+/-}$	Franco et al., 2014	N/A
Mouse: BALB/c NeuT/*Pik3c2a*$^{+/-}$	This paper	N/A
Oligonucleotides		
Pik3c2a Sh1: GGCAAGATATGTTAGCTTT	Thermo Scientific	Cat. # V2LMM_73461
Pik3c2a Sh2: CAAAGTTTCTTTAACTCT	Thermo Scientific	Cat. # V2LMM_66190
siRNA: *PIK3C2A*, GGAUCUUUUUAAACCUAUU (#1),	Dharmacon	N/A
siRNA: *PIK3C2A*, ACACCTGTATTACCAGTTA (#2)	Dharmacon	N/A
siRNA: TACC3 5'CAGUUUGGAACUUCCUCGU3'	Santa Cruz Biotechnology	Cat. # sc62578
siRNA: MAD1	Santa Cruz Biotechnology	Cat. # sc62578
siRNA: MAD2	Santa Cruz Biotechnology	Cat. # sc35838
sgRNAs for CRISPR/Cas9 mediated silencing of *PIK3C2A* sgRNA #1 Fwd CACCGAGCATTACAGATGGAAGCAGAGG	This paper	http://crispr.mit.edu
sgRNA #1 Rev AAACCCTCTGCTTCCATCTGTAATGCTC	This paper	http://crispr.mit.edu
sgRNA #2 Fwd CACCGTCCACATCTTTTGCTCTTGTTGG	This paper	http://crispr.mit.edu
sgRNA #2 Rev AAACCCAACAAGAGCAAAAGATGTGGA	This paper	http://crispr.mit.edu
Pik3c2a wild-type allele: AAGATGTGAACAAAGCAGAAGCGTTAC	Sigma	N/A
Pik3c2a wild-type allele ACTGACTAGTGGCCGATAGACTGGTAAAC	Sigma	N/A
Pik3c2a knockout allele: AAGATGTGAACAAAGCAGAAGCGTTAC	Sigma	N/A
Pik3c2a knockout allele TATGCAGCAACGAGACGTC	Sigma	N/A
Recombinant DNA		
pBrain-GFP-FKBP-TACC3-shTACC3	gift from S. Royle	Addgene plasmid # 59354
PI3K-C2α-GFP (Δ1–380)	This paper	N/A
PI3K-C2α-GFP (Δ1–512)	This paper	N/A
PI3K-C2α-GFP (Δ1–670)	This paper	N/A
PI3K-C2α-GFP (Δ1–830)	This paper	N/A
PI3K-C2α-GFP (512-670)	This paper	N/A
PI3K-C2α-FLAG (Δ1–380)	This paper	N/A
PI3K-C2α-FLAG (Δ1–512)	This paper	N/A
PI3K-C2α-FLAG (Δ1–670)	This paper	N/A
PI3K-C2α-FLAG (Δ1–830)	This paper	N/A
PI3K-C2α-GFP	gift from M. Falasca	N/A
PI3K-C2α KD	Franco et al., 2014	N/A

CONTACT FOR REAGENT AND RESOURCE SHARING

Further information and request for resources and reagents should be directed to the lead contact: Emilio Hirsch (emilio.hirsch@unito.it).

EXPERIMENTAL MODEL AND SUBJECT DETAILS

Animals

BALB/c *Pik3c2a*$^{+/-}$ mice were previously generated (Franco et al., 2014). Mutant mice were crossed for 10 or more generations with breast cancer mouse model overexpressing the activated form of Neu oncogene (BALB/c rHER-2/NeuT) in the mammary gland(Quaglino et al., 2004). *WT/NeuT* mice were used as controls. Only individually tagged virgin female mice were used. All experiments were carried out according to the European Community guiding principles in the care and use of animals. All animal experiments were authorized by the Italian Ministry of Health (authorization number 856/2015-PR) and carried out according to the European Community guiding principles in the care and use of animals.

Human Subjects

To assess the clinical relevance of PI3K-C2α expression to breast cancer, we analyzed a series of 1779 operable breast cancer patients, available on tissue microarray (TMA), who underwent surgery at the European Institute of Oncology (IEO) in Milan from years 1997 to 2000. Complete clinico-pathological and follow-up information were available for all the patients. The median length of follow-up was 14.1 years. The study was approved by the Institutional Review Board of the European Institute of Oncology (Milan, Italy) and informed consent was obtained from all subjects.

To assess the value of PI3K-C2α expression as a predictive biomarker of therapy response, we used a series of 43 breast cancer core biopsies of patients treated with Taxane-based chemotherapy in the neoadjuvant setting was retrieved from the pathology files of the Candiolo Cancer Institute IRCCS, Candiolo, Italy. Patients characteristics are available in Table S5. Pathological response on surgical specimens was categorized following (Pinder and Reis-Filho, 2007) in pathological complete response (pCR) if no residual invasive tumor was found, in situ carcinoma may be present, pathological partial response (pPR) if residual disease or minor signs of response were present on the surgical specimens compared to the tumor cellularity of the pre-treatment core biopsies, pathological non-response (pNR) if no evidence of response to therapy was detected (the presence of lymph node metastasis was not taken into account) (Balmativola et al., 2014; Pinder and Reis-Filho, 2007). With regard to the definition of molecular subtypes, we referred to the St. Gallen recommendations (Coates et al., 2015; Goldhirsch et al., 2007, 2011). The study was approved by the Comittee for human Biospecimen Utilization (DSM-ChBU) of the Department of Medical Sciences, University of Turin, Italy, and informed consent was obtained from all subjects.

Cell Lines and Primary Cultures

Tumors of different size were collected from BALB-WT/NeuT and BALB-Het/NeuT mice. Tumors were finely chopped and then digested in DMEM medium (Gibco®), containing 1 mg/ml collagenase A (Roche Applied Science, Indianapolis, IN, USA). After 30 min at 37°C, a mixture of epithelial-enriched fragments and non-epithelial single cells was obtained. The epithelial-enriched fraction, resulting from filtration through a 70 micron mesh (BD), was digested with 0.025% trypsin-EDTA (Gibco®), centrifuged at 1200 rpm for 5 min and plated on 10-cm dish. Cells were treated with 0.025% trypsin-EDTA (Gibco®) until fibroblasts elimination and cultured in DMEM High Glucose GlutaMAXTM (Gibco®) 20% Fetal Bovine Serum (Invitrogen) supplemented with 5000 U/ml Penicillin-Streptomycin (Gibco®), 1 mM Sodium Pyruvate (Gibco®) and MEM Non-Essential Amino Acids (Gibco®). Six independent Murine Mammalian Epithelial Tumor (MMET) cells were used. Cells were detached using 0.1% trypsin-EDTA (Gibco®). Primary MEFs were obtained from E11.5 day-old embryos (Franco et al., 2014). Cells were kept in culture for no longer than 10 days, with the exception of fast-growing adapted populations of MEFs.

HeLa, HEK293T, MCF10A, MCF7, BT474, SKBR3 and T47D female cell lines were purchased from ATCC (without further authentication) and cultured in DMEM GlutaMAXTM medium supplied with 10% fetal bovine serum (FBS) and 1% Penicillin-Streptomycin (10,000 U/mL). Cell lines used in this paper are not listed in the database of commonly misidentified cell lines maintained by ICLAC. Cell lines are routinely tested for mycoplasma contamination.

METHOD DETAILS

Analysis of Mice

To evaluate tumor appearance, all mammary glands were inspected weekly, beginning after the 8 weeks of age. The development of neoplastic lesion was performed in the fourth set of mammary glands. When tumors were detectable by palpation, neoplastic masses were measured weekly with calipers in two perpendicular diameters and the average value recorded after each examination. Tumor volume was calculated using the following formula: $d*D^2/2$, where d stands for minor diameter and D for major diameter. Progressively growing masses greater than 2 mm mean diameter were regarded as tumors. Tumors were defined "early" when $2<D<4$ mm (tumor mass no larger than 70 mm^3) and "late" when $D>6$ mm (tumor mass >100 mm^3).

Differences in tumor incidence were evaluated with Mantel-Cox log-rank test and differences in tumor multiplicity with Student's *t* test. Tumor multiplicity was calculated as the cumulative number of incident tumors per total number of mice.

For orthotopic injections, WT/NeuT and Het/NeuT MMET cells (10^6 cells) were injected in left and right fat pad of 8 weeks old *Pik3c2a*$^{+/+}$ mice. NSG mice (6-8-week-old) were injected subcutaneously (orthotopic) with 1×10^6 cells (SKBR3) or 5×10^6 MCF-7 on day 0. For MCF-7, cells were resuspended in 50% Matrigel (BD Biosciences) before sub-cutaneous injection in NSG mice. Slow release oestrogen pellets were implanted sub-cutaneously into mice two days before cell injection. About 2-4 weeks after inoculation, when the tumor reached an average volume of 70 mm^3, mice were randomized and divided into four groups (Paclitaxel, doxorubicin, combination, control). Paclitaxel (10461, Cayman Laboratories) was given 10 mg/kg, IP for 14 days (Day 1, 4, 8, 11, 14). Doxorubicin (Sigma) was given by intravenous injection each third day (six times) for 14 days at 1 mg/kg per day. The control group was treated with vehicle.

All mice were killed two weeks after the end of treatment or when the tumor mass was >1500 mm^3. Tumor masses, lymph nodes, lungs and livers were collected for histological analysis.

All experiments on mice have been performed in accordance with institutional and national guidelines and they conform to the relevant regulatory standards.

The investigators were not blinded during experiments and outcome assessment.

Histopathological Analysis

For histological analysis, mammary glands were fixed overnight in 4% paraformaldehyde (PFA), embedded in paraffin and cut into 3 μm thick sections. Sections were stained with hematoxylin and eosin (H&E) following standard protocols and with specific antibodies. For protein proliferating cell nuclear antigen (PCNA, PC-10 sc-56, Santa Cruz Biotecnology) staining, slides were subjected to antigen retrieval with citrate buffer, the antibody (diluted 1:200) was localized by M.O.M kit (Vector Laboratories) and signal was detected with 3,3′-Diaminobenzidine (DAB) liquid substrate system tetrahydrochloride (Sigma-Aldrich). Slides were counterstained in eosin, dehydrated and mounted with moviol. Randomly selected areas where investigated under the light microscope (Olympus BH2), micro-photographed through digital imaging system then analyzed with ImageJ software. Apoptotic cells were detected by terminal deoxynucleotidyl transferase (TdT)-mediated dUTP nick end labeling (TUNEL) reaction (R&D Systems). Quantitative studies of immunohistochemically stained sections were performed in a blinded fashion. Sections were analyzed on an Olympus BH2 microscope (objective Olympus Plan10×), equipped with an Olympus DP50 camera for images acquisition. For murine whole-mount analysis, fresh mammary tissue was flattened and fixed in Carnoy's solution (ethanol, glacial acetic acid, and chloroform) and subsequently stained with carmine alum (Quaglino et al., 2004).

Cell Culture and Proliferation

For proliferation assays via cell counts, MEFs and MMET cells were plated into 96-well plates in octuplicate at 4×10^3 cells/well and counted with a 3-(4,5-dimethyl thiazol-2-yl)-2,5-diphenyl tetrazolium bromide–based colorimetric assay (MTT) (Roche, Germany). Absorbance was recorded at days 1, 2, 3, 4, 5, 6, 7 and 8 for MEFs and days 2, 4, 6 and 8 for MMET.

For drug treatment, cells were seeded in octuplicate at 4×10^3 cells per 96-well plate; Paclitaxel and/or Doxorubicin were added the day after seeding in DMEM High Glucose GlutaMAX^{TM} (Gibco®) 5% Fetal Bovine Serum (Invitrogen) supplemented with 5000 U/ml Penicillin-Streptomycin (Gibco®), 1 mM Sodium Pyruvate (Gibco®) and MEM Non-Essential Amino Acids (Gibco®). Cells were counted 24 hours after drug treatment with a 3-(4,5-dimethyl thiazol-2-yl)-2,5-diphenyl tetrazolium bromide–based colorimetric assay (Roche, Germany). Cell survival was considered as the ratio of live cells after treatment compared with live cells treated with vehicle alone.

For MPS1 inhibition, 100 nM of NMS-P715 (475949, Calbiochem) was added the day after seeding for 48 hours.

Cell Synchronization

MMET, MEF, HEK293T and HeLa cells were synchronized in metaphase using 2 mM thymidine (Sigma-Aldrich) for 20 hours, 30 μM deoxicitidine for 6 hours (Sigma-Aldrich) and 50 ng/ml of nocodazole (Sigma-Aldrich) for 12 hours, followed by 2 hours release in fresh medium in the presence of 20 μM MG132 (Calbiochem). HeLa cells were blocked in interphase by starvation for 16 hours.

Flow Cytometry Analysis

For DNA content determination, cells were seeded at 4×10^5 cells per 6-cm dish in triplicate. The day after seeding, cells were starved for 18 hours. Cells were detached with 0.1% trypsin-EDTA (Gibco®), fixed in ethanol 70% overnight at -20°C and stained 40 min at 37°C with PI solution, containing 0.05% Triton X-100, 0.1 mg/ml RNase and 25 μg/ml Propidium Iodide (P4864, Sigma-Aldrich).

To determine the mitotic checkpoint status, cells were treated with 100 ng/ml nocodazole (Sigma-Aldrich) for 16 hour, followed by DNA content determination.

For Annexin V staining, cells were seeded at 4×10^5 cells per 6-cm dish in triplicate. Cells were starved 48 hours after seeding and Annexin V (556419, BD) staining was performed according standard protocol. Sample were analyzed using a FACSCalibur flow cytometer (Becton Dickinson Immunocytometry Systems, San Jose, USA). Doublets were excluded by cell size and fluorescence intensity.

CRISPR/CAS9

For CRISPR/Cas9 mediated silencing, target sequences were designed via a gRNA design tool (Feng Lab CRISPR Design Web Tool at http://crispr.mit.edu). Each sequence was cloned into the PX335 plasmid to express the Cas9n (nickase) and two single guide RNAs (sgRNAs) were then co-trasfected in HEK293T cells to delete *PIK3C2A* gene.

Plasmids

All constructs were verified by restriction digest and automated DNA sequencing. HEK293T cells were transfected using calcium phosphate. MMET and HeLa cells were transfected by lipofection using Lipofectamine® 2000 (Life Technologies), according to the manufacturer's instructions. Doxycycline-inducible clathrin heavy chain (CHC) knockdown HeLa cells were cultured in MEM supplemented with 10% South America FBS (Euroclone), 1 mM Sodium Pyruvate (Gibco®), MEM Non-Essential Amino Acids (Gibco®), and 400 μg/ml G418 (Gibco®). HeLa cells were treated with doxycycline (0.5 μg/ml) for 7 days to achieve a >80% decrease of CHC levels.

Immunofluorescence

Immunofluorescence was performed by ice cold methanol fixation of MEF, MMET and HeLa cells followed by standard procedures(Franco et al., 2014). For PI3K-C2α staining the following protocol was used: HeLa cells were permeabilized with 0,1% Saponin for 10 seconds and then fixed in 2% PFA for 5 minutes. After two washes in PBS containing 0,1% Saponin, cells were blocked in PBS 0,1% Saponin and 2% BSA for 20 minutes. For endogenous detection of PI3K-C2α the Proteintech 22028-1-AP antibody was used at a concentration of 1:500 in blocking solution containing PBS 0,1% Saponin and 2% BSA for 1 hr. To detect the GFP- PI3K-C2α in transfected cells, anti GFP antibody (a generous gift from E. Turco)(Franco et al., 2014) was used in blocking solution for 45 minutes. Alexa secondary antibody (Alexa 488, Alexa 568 or Alexa633) were used 1:1000 for 45 minutes. Cells were stained with DAPI and examined with either Zeiss Observer-Z1 microscope, equipped with the Apotome, Leica TCS-II SP5 or Leica TSC-II SP8 confocal microscope. Raw images were digitally processed only to normalize the background and enhance the contrast. Z-stacks were acquired and processed with the Maximum Projection tool. 3D morphometric measurement and reconstruction was performed with Imaris (BitPlane, Zurich, Switzerland). To assess CHC, TACC3, PI3K-C2α and ch-TOG abundance on the spindle, fluorescence intensity was calculated with ImageJ tools and normalized on tubulin and background fluorescence in accordance with standard methods (Burgess A et al, PNAS 2010; McCloy RA, et al Cell Cycle). At least 25 photo/genotype were taken in four independent experiments. Metaphase spindle length (the maximum distance between γ-tubulin positive spindle poles) (Fu et al., 2015), (Luo et al., 2016)and metaphase plate width (the maximum projection of DAPI positive stacks) was assessed using ImageJ distance measurement tools.

Protein Analysis

Cells were homogenized in lysis buffer (120 mM NaCl, 50 mM Tris-HCl pH=8, 1% Triton X-100) supplemented with 25x protease inhibitor cocktail (Roche), 50 mM sodium fluoride and 1 mM sodium orthovanadate. Lysates were cleared by centrifugation at 13,000 rpm for 15 min at 4°C. Protein concentration was determined by Bradford method and supernatants were analyzed for immunoblotting or for immunoprecipitation (IP) with the indicated antibodies. Membranes probed with the indicated antibodies were then incubated with HRP conjugated secondary antibodies (anti-mouse used 1:10000, anti-rabbit 1:5000, Sigma) and developed with enhances chemiluminescence (ECL, BD).

For IP assays, mitotically arrested cells were used. 1 mg of pre-cleared extracts were incubated with 1 μg of the indicated antibody at 4°C on a rotating rack. After 1,5 hours, 15 μl of protein G-Sepharose (Amersham Biosciences, Buckinghamshire, UK) were added for 30 minutes. Samples were collected by centrifugation (13000 rpm 1 min) and washed six-times with lysis buffer. Bound protein complexes were then eluted by adding 30 μl Laemmli sample buffer. Spindle fractionation on HeLa and HEK293T cells was performed by incubation in a series of 4 buffers (Booth et al., 2011), followed by collection of pellets each time by centrifugation at 1000 × g for 4 min at room temperature and resuspension in the following buffer (Booth et al., 2011).

For pull-down experiment, HEK293T cells were transfected with GFP vector, PI3K-C2α-GFP WT or PI3K-C2α-GFP 512-670. 24 hours after transfection, cells were harvested and homogenized in lysis buffer (120 mM NaCl, 50 mM Tris-HCl pH=8, 1% Triton X-100) supplemented with 25x protease inhibitor cocktail (Roche), 50 mM sodium fluoride and 1 mM sodium orthovanadate. Lysates were cleared by centrifugation at 13,000 rpm for 15 min at 4°C. 1 mg of pre-cleared extracts were incubated with 1 μg of anti-GFP (ab1218, Abcam) and 15 μl of protein G-Sepharose for 2 hours at 4°C on a rotating rack. Samples were collected by centrifugation (13000 rpm 1 min) and washed six-times with lysis buffer. Bound protein complexes were resuspended in 500 μl of reaction buffer (50 mM Hepes pH=7.5, 100 mM NaCl, 0.05% Triton X-100, 2 mM DDT, 3 mM MgCl$_2$, protease inhibitors) and incubated with 1 μg FLAG-TACC3 (TP310754, OriGene) for 1 hour at 4°C on a rotating rack. Samples were collected by centrifugation (13000 rpm 1 min) and washed six-times with reaction buffer. Bound protein complexes were then eluted by adding 30 μl Laemli sample buffer.

For *in vitro* binding, equimolar amount of 1 μg GST-PI3K-C2α (SRP5330, Sigma) or 140 ng GST was incubated with 15 μl of protein G-Sepharose for 30 minutes at 4°C in 500 μl of reaction buffer (50 mM Hepes pH=7.5, 100 mM NaCl, 0.05% Triton X-100, 2 mM DDT, 3 mM MgCl2, protease inhibitors), after which 1 μg FLAG-TACC3 (TP310754, OriGene) was added for 30 minutes. Beads were washed four times with 1 ml of reaction buffer and analyzed by Western blotting after the addition of 30 μl of Laemmli.

Metaphase Spread Preparation and Telomere-FISH (T-FISH) Analysis

Cell suspensions were incubated in Colcemid (KaryoMAX Colcemid Solution; GIBCO) at the final concentration of 50 ng/mL for 3–5 hours. Metaphase spreads were prepared according to standard protocols (Franco et al., 2006). For T-FISH analysis, a FISH assay that combines DAPI staining with a Cy3-labeled telomere-specific peptide nucleic acid (PNA) probe (Cy3-[TTAGGG]3) (Applied Biosystems) was employed to assay metaphase chromosomes for instability (Franco et al., 2006). Metaphases images were acquired with BX61 Microscope (Olympus) equipped with a motorized automatic stage, a cooled-CCD camera, an interferometer (Applied Spectral Imaging), and a 633 objective lens. Analysis was performed with the HiSKY software (Applied Spectral Imaging).

Cold-Treatment Stability Assay

HeLa cells were grown in Dulbecco's modified medium (DMEM) containing 10% FCS, 100 U/ml penicillin, 100 mg/ml streptomycin at 37°C with 5% CO_2 in a humidified incubator. Cells were transfected with PI3K-C2α siRNA or control (scramble) siRNA using lipofectamine RNAiMAX (Invitrogen) for 48 hours. Transfected cells were placed on ice and incubated in ice cold medium for 10 minutes, rinsed with cytoskeleton buffer (10 mM MES, 150 mM NaCl, 5 mM glucose, 5 mM MgCl2,) before fixing with 3% formaldehyde, 0.1% Triton X-100, and 0.1% glutaraldehyde for 15 min (Gasic et al., 2015). Cells were rinsed again with cytoskeleton buffer and stained with mouse anti-α-tubulin (1:10000, Sigma-Aldrich) and cross-adsorbed secondary antibodies (Invitrogen). To evaluate the stability of K-fibers, images of mitotic cells were collected in 2.0 μm steps using a 60x 1.4 NA objective on an inverted Nikon Eclipse Ti-E microscope equipped with a DAPI/FITC/TRYC3 filter set and a Hamamatsu Flash 4.0 SCMOS camera, and the images recorded with Nikon Imaging Software Advanced research (NIS AR).

Breast Cancer Patients

To assess the clinical relevance of PI3K-C2α expression to breast cancer, we analyzed a series of 1779 operable breast cancer patients, available on tissue microarray (TMA), who underwent surgery at the European Institute of Oncology (IEO) in Milan from years 1997 to 2000. Complete clinico-pathological and follow-up information were available for all the patients. The median length of follow-up was 14.1 years. The study was approved by the Institutional Review Board. Immunohistochemical staining was performed in a Bond Max Automated Immunohistochemistry Vision Biosystem (Leica Microsystems GmbH, Wetzlar, Germany) using the Bond Polymer Refine Detection Kit (DS9800). Three-μm-thick sections were prepared from formalin-fixed paraffin-embedded (FFPE) TMA tissue blocks, deparaffinized, pre-treated with the Epitope Retrieval Solution 1 (pH 6.0) at 100°C for 20 min and then incubated for 30 min with a anti-PI3K-C2α antibody (OriGene TA801690) diluted at final concentration of 1 μg/ml in Bond Primary Antibody Diluent (AR9352). TMA slides were acquired with the Aperio ScanScope system (Leica Microsystems GmbH, Wetzlar, Germany). The intensity of PI3K-C2α expression was scored from 0 to 3 (scoring categories 0, 0.5, 1, 1.5, 2, 2.5 and 3).

To assess the value of PI3K-C2α expression as a predictive biomarker of therapy response, we used a series of 43 breast cancer core biopsies of patients treated with Taxane-based chemotherapy in the neoadjuvant setting was retrieved from the pathology files of the Candiolo Cancer Institute IRCCS, Candiolo, Italy. Patients characteristics are available in Table S5. Pathological response on surgical specimens was categorized following Pinder et al.(Pinder and Reis-Filho, 2007)in pathological complete response (pCR) if no residual invasive tumor was found, *in situ* carcinoma may be present, pathological partial response (pPR) if residual disease or minor signs of response were present on the surgical specimens compared to the tumor cellularity of the pre-treatment core biopsies, pathological non-response (pNR) if no evidence of response to therapy was detected (the presence of lymph node metastasis was not taken into account) (Balmativola et al., 2014; Pinder and Reis-Filho, 2007). With regard to the definition of molecular subtypes, we referred to the St. Gallen recommendations (Coates et al., 2015; Goldhirsch et al., 2007, 2011). Three micron thick sections of formalin fixed paraffin embedded (FFPE) samples were stained for haematoxylin and eosin (H&E) and immunohistochemistry with antibodies against PI3K-C2α (clone OTI15H1, formerly 15H1, diluted 1:1000, Origene). Immunohistochemistry was performed using an automated slide-processing platform (Ventana BenchMarck XT Autostainer, Ventana Medical Systems). Positive and negative controls were included for each immunohistochemical run. The antibody was optimized on FFPE cell block sections of knocked down (shRNA and scramble ctrl) HeLa cells and on a series of normal tissue samples including breast, kidney, thyroid, lymph-nodes, lung, colon. IHC scoring was based on basal staining intensities of PI3K-C2α expression in the normal breast (epithelial cells and stromal compartment) leading to a four-tier scoring system ranging from score 3 (high intensity), score 2 (moderate staining intensity, comparable to normal tissue), score 1 (reduction in staining intensity compared to normal tissue), score 0 (absence of PI3K-C2α staining with positive internal control). The study was approved by the Comittee for human Biospecimen Utilization (DSM-ChBU) of the Department of Medical Sciences, University of Turin, Italy. Patients received Paclitaxel concurrently prior to surgery as indicated as follows: doxorubicin 50 mg/m2 plus Paclitaxel 175 mg/m2 once every 3 weeks for 6 cycles, 43 patients); HER2 positive (IHC 3+ or amplified FISH) patients, in addition to the above treatment, received Trastuzumab (Herceptin) once every 3 weeks for 4 cycles.

QUANTIFICATION AND STATISTICAL ANALYSIS

General Experimental Approaches

All of the statistical details of experiments can be found in the figure legends, in the Results and the STAR Methods sections, including the statistical tests used, exact value of n, what n represents (number of animals, cells, patients, experiments) and precision measures (mean, median, SD, SEM, confidence intervals). No statistical methods were used to predetermine sample size. No

samples, mice or data points were excluded from the reported analyses. Samples were not randomized to experimental groups. Sample size (number of mice) was determined on the basis of our previous studies (Franco et al., 2014, 2015). The investigators were not blinded to allocation during experiments and outcome assessment.

Statistical Analysis

Prism software (GraphPad) was used for statistical analysis. Significance was calculated with Student t test and one- or two-way analysis of variance tests (ANOVA) followed by Bonferroni's post hoc analysis, or Mantel Cox log-rank test where appropriate. Values are reported as the mean ± standard error of the mean (SEM). For statistical analysis in breast tissue samples, we used contingency tables with Fisher's exact test or Chi square test. $p < 0.05$ was considered statistically significant (*), $p < 0.01$ very significant (**) and extremely significant $p < 0.001$ (***).

Distant metastasis (DM) was defined as the time from surgery to the appearance of a local or regional recurrence and distant metastasis or death from breast cancer as a first event, respectively(Hudis et al., 2007). Second primary cancer or death from unknown cause or other cause were considering as competing events. For the IEO cohort, the hazard ratios (HR) of DM events in the comparison of high vs low PI3K-C2α tumors both by univariate and multivariable analyses were estimated with Cox proportional hazards models. Multivariable models were adjusted for Grade, Ki-67, HER2 status, estrogen/progesterone status, tumor size, number of positive lymph nodes and age at surgery if available. PI3K-C2α protein status was categorized in low and high according to IHC score ≤ 1.0 or > 1.0, respectively. Categorical data derived from (Hatzis et al., 2011; Martin et al., 2011)and IRCCS cohort were compared using chi-sq. or Fisher's exact test to estimate the effects of PI3K-C2α expression on response to neoadjuvant therapy. Agresti and Coull (modified Wald method) was used to calculate 95% confidence interval.

Gene Expression Data Sets

We obtained raw microarray expression data for breast cancer cohorts from (Martin et al., 2011) and (Hatzis et al., 2011). Expression of PI3K-C2α was scored as "high" or "low" using the median value as threshold. Data from Table S5 are publicly available for download through the cBioPortal for Cancer Genomics (http://www.cbioportal.org).